Journal of Cleaner Production 552 (2026) 147949

Contents lists available at ScienceDirect

Journal of Cleaner Production

journal homepage: www.elsevier.com/locate/jclepro

Hydrogen-driven co-production of Portland clinker precursor and methanol: A sustainable CO_2 mitigation strategy

Dongliang Zhang [a], Hanke Li [b], Qiangqiang Wu [c], Xiangdong Yu [a], Hao-Fan Wang [a], Yonghai Cao [a], Hongjuan Wang [a], Siyu Yang [a,*], Hao Yu [a,**]

[a] School of Chemistry and Chemical Engineering, Guangdong Provincial Key Lab of Green Chemical Product Technology, South China University of Technology, Guangzhou, 510641, China
[b] National Reference Laboratory for Food Contact Material (Guangdong), Guangzhou Customs Technology Center, Guangzhou, 510075, China
[c] School of Engineering, Guangzhou College of Technology and Business, Foshan, 528138, China

HIGHLIGHTS

- Low-carbon Portland clinker precursor processes are modeled.
- Adopt coke oven gas and pure H_2 to calcine raw meal, integrating syngas-to-methanol to reduce CO_2.
- Coke oven gas-driven configuration enables cross-industry synergy: steel, cement, and chemical.
- Fossil hydrogen and green hydrogen from selective biomass gasification or wind-photovoltaic (<3.74 $/kg) offer compelling economic advantages.

GRAPHICAL ABSTRACT

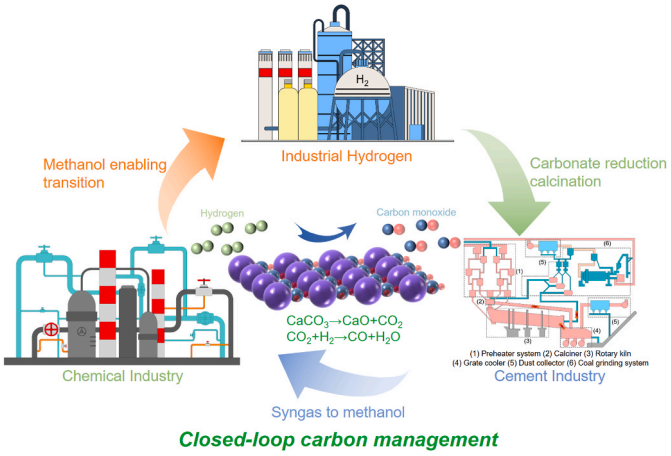

ARTICLE INFO

Keywords:
Carbonate Reduction Calcination
Cross-Industry Carbon Utilization
Portland Clinker Precursor
Methanol
Techno-Economic Analysis

ABSTRACT

The cement industry faces a critical decarbonization challenge, with over 60% of sectoral emissions arising from high-temperature calcination of limestone, according to the study by Montes-Hernandez in 2025. This emission source is intrinsically linked to cement chemistry and remains inadequately addressed by existing technologies. This study proposes an innovative co-production of Portland clinker precursor and methanol *via* carbonate reduction calcination, enabling cross-industry carbon utilization and source-level carbon dioxide (CO_2) mitigation. A comprehensive techno-economic analysis is conducted on the proposed processes driven by coke oven gas (COG) and pure H_2 to evaluate their environmental and economic performance. When pure H_2 is supplied *via* steam methane reforming, selective biomass gasification, or wind–photovoltaic coupled water electrolysis (price <3.74 US dollar per kg H_2), the H_2-driven configuration is economically viable and exhibits outstanding

* Corresponding author.
** Corresponding author.
E-mail addresses: cesyyang@scut.edu.cn (S. Yang), yuhao@scut.edu.cn (H. Yu).

https://doi.org/10.1016/j.jclepro.2026.147949
Received 24 October 2025; Received in revised form 28 February 2026; Accepted 6 March 2026
Available online 12 March 2026
0959-6526/© 2026 Elsevier Ltd. All rights are reserved, including those for text and data mining, AI training, and similar technologies.

environmental performance, with a carbon utilization efficiency of 99.74%, a levelized energy consumption of 8.51 GJ per tonne Portland clinker precursor, and a levelized CO_2 emission of 0.29 tonne CO_2 per tonne Portland clinker precursor (LCEOP). In contrast, the COG-driven configuration exhibits a higher LCEOP, at 0.55 tonne CO_2 per tonne Portland clinker precursor, but delivers superior economic performance, with a net present value of 134.17 million US dollars, an internal rate of return of 16.01%, and a dynamic payback period of 11.84 years. Sensitivity analysis indicates that the COG-driven configuration has strong resilience to price volatility, while it further facilitates the systematic integration of steel, cement, and chemical industries.

1. Introduction

Since the invention of Portland cement in the early 19th century (ACA, 2025), Global cement output has been persistently increasing due to population growth, accelerated urbanization, and extensive infrastructure development, which is projected to reach 4 billion tonnes by 2050 (IEA, 2025). Carbon dioxide (CO_2) emissions permeate various stages of cement production process, where over 60% originates from calcination of carbonate minerals (Montes-Hernandez, 2025). Current decarbonization technologies focus on the following approaches: (*i*) Energy efficiency enhancement (Amiri and Vaseghi, 2015; Boháč et al., 2022; Marenco-Porto et al., 2023; Matsuzawa et al., 2017; Okoji et al., 2022; Sanaye et al., 2020); (*ii*) Raw material substitution (Chen et al., 2010; Goncharov and Zhutovsky, 2022; Her et al., 2022; Ryu et al., 2024; Tsakiridis et al., 2016; Wang et al., 2020); (*iii*) Fuel substitution (Bourtsalas et al., 2018; Huang et al., 2017; Jacob and Tokheim, 2023; Karpan et al., 2022; Tsakiridis et al., 2017; Williams et al., 2024); (*iv*) End-of-pipe carbon capture, utilization and storage (CCUS) deployment (Bacatelo et al., 2023; Gallego Dávila et al., 2023; Wang et al., 2024); (*v*) Novel process development (Ellis et al., 2020; Zhang et al., 2022).

While the aforementioned approaches can effectively mitigate CO_2 emissions from cement manufacture, the industry's inherent characteristics of high production capacity and narrow profit render economically prohibitive. Carbonate minerals (e.g., limestone, dolomite) constitute virgin raw materials for cement manufacture, while simultaneously serve as the Earth's predominant carbon reservoirs. Their massive global reserves significantly influence the biospheric carbon cycle. H_2-driven conversion of carbonates into platform chemicals facilitates closed-loop carbon management through synergistically coupling with the chemical industry, thus enabling structural upgrading of the cement industry. Techno-economic analysis (TEA) provides a quantitative framework by integrating energy consumption, raw material cost, and potential carbon tax, enabling the assessment of both economic viability and environmental sustainability of H_2-driven carbonate reductive calcination in the context of coupled cement and chemical industries. Although previous studies have focused primarily on experimental investigations, system-level, process-oriented research remains limited. Pioneering studies by Giardini et al. (1968) and Reller et al. (1987) demonstrated that catalytic hydrogenation of alkaline earth carbonates and alkaline earth-transition metal composite carbonates into C_xH_y realizes the direct synthesis of organic carbon from inorganic carbonates. Sun et al. (2024) evaluated the performance of potassium-promoted CaO as a dual-functional sorbent/catalyst over 50 integrated carbon capture and utilization cycles at 650 °C, which allowed approximate 100% CO_2 capture efficiency during carbonation and effectively bypassed the thermodynamic limitations of conventional gas-phase CO_2 hydrogenation, achieving >95% CO_2-to-CO conversion and ~100% CO selectivity. Wang et al. (2023) employed micro-fluidized bed thermogravimetric analysis coupled with mass spectrometry and *in situ* measurements to investigate limestone decomposition under H_2 and Ar atmospheres. Their results represented that H_2 atmosphere increased the limestone decomposition rate by 5-fold (79.1% CO_2-to-CO conversion and ~100% CO selectivity at 710 °C) compared to Ar. Xue et al. (2023) further reported the co-thermal *in situ* reduction of $CaCO_3$ under pure H_2 at 750 °C, with a CO selectivity of 93.7% and a CO formation rate up to 0.756 mmol/min. Integration of green hydrogen generated from electrochemical water splitting powered by renewable energy (Eq. (1)) with carbonate reduction calcination (Eq. (2)) enables source-level decarbonization without additional energy input. Moreover, the downstream conversion of syngas (e.g., CH_3OH) (Eq. (3)) serves as a critical nexus linking the cement industry with the CO_2-derived chemical industry, thereby enabling synergistic carbon utilization pathways. However, economic viability remains strongly dependent on H_2 price, necessitating scalable low-cost hydrogen donor for industrial competitiveness.

$$2H_2O \rightarrow 2H_2 + O_2 \quad (1)$$

$$CaCO_3 + H_2 \rightarrow CaO + CO + H_2O \quad (2)$$

$$2H_2 + CO \rightarrow CH_3OH \quad (3)$$

Apart from H_2, CH_4 has emerged as a promising and cost-effective hydrogen donor for carbonate reduction calcination. Compared with H_2, CH_4 exhibits several advantages, including abundant reserves, ease of transportation, and less safety hazards. Nikulshina et al. (2009) conducted an exploratory experiment in a 5 kW solar-driven chemical reactor, achieving 83% $CaCO_3$ conversion and 38% CH_4 conversion during 11 min of irradiation at a solar concentration ratio of 1884 suns and a nominal temperature of 950 °C. Zhang et al. (2025) demonstrated the feasibility of direct reduction of $CaCO_3$ by CH_4 in the presence of a highly dispersed NiO/S-1 catalyst. Shao et al. (2024) developed a Ni/CaO catalyst for the $CaCO_3$-CH_4 dry reforming using cement raw meal at 700 °C, achieving 95% CaO yield, 91% syngas selectivity, and 90% CH_4 conversion. Process simulation and economic analysis indicate that this approach can reduce 37.2% CO_2 emissions in comparison with the conventional $CaCO_3$ thermal decomposition and achieve 271.0 US dollar per tonne clinker net profit. Wang et al. (2024) proposed a new cement process that combines $CaCO_3$-CH_4 dry reforming with syngas-to-methanol, integrating the organic Rankine cycle and carbon capture and storage, achieving 194 kg CO_2-equivalent per tonne clinker of environmental performance. Jiang et al. (2023) found that a H_2-to-CH_4 feed ratio of 1:1 or higher can effectively suppress carbon deposition while enabling complete decomposition of $CaCO_3$. These findings indicate that alternative hydrogen sources should be carefully considered: the direct utilization of biogas (primarily composed of CH_4 and CO_2) for the reduction calcination of cement raw meal would likely exacerbate carbon deposition and compromise long-term operational stability, whereas ammonia requires additional conversion steps to generate usable hydrogen, substantially increasing process complexity.

The above studies confirm that employing CH_4-rich hydrogen sources (e.g., coke oven gas (COG)) (H_2-to-CH_4 feed ratio of 2.27) (Table S1, ESI†)) in carbonate reduction calcination not only enhances syngas output (Eqs. (2) and (4)) but also delivers superior economic and environmental performance. At the policy level, the EU Carbon Border Adjustment Mechanism (EEAS, 2025) has brought carbon-intensive industrial products, such as cement and steel, under its regulatory scope, whereby the carbon intensity of production processes directly influences enterprises' market competitiveness. Meanwhile, China's hydrogen development roadmap (NDRC, 2022) identifies green H_2 as a long-term strategic objective, while explicitly emphasizing the need to effectively utilize industrial by-product hydrogen and other hydrogen-rich resources during the transition period. Against this industrial and policy landscape, treating COG as a transitional pathway for collaborative

decarbonization and green H_2 as a long-term pathway for deep decarbonization enables a comparative assessment that clarifies the trade-offs between transitional mitigation options and long-term deep decarbonization strategies, thereby ensuring both practical relevance and policy significance.

$$CaCO_3 + CH_4 \rightarrow CaO + 2CO + 2H_2 \quad (4)$$

To develop an economically and environmentally preferred process, this study proposes an integrated process that couples carbonate reduction calcination with syngas-to-methanol, enabling co-production of Portland clinker precursor (highly reactive CaO—a key intermediate for Portland clinker) and methanol. The proposed process further incorporates gas-steam combined cycle to maximize process waste heat utilization, thereby enhancing overall energy conversion efficiency. The effective utilization of metallurgical byproduct COG establishes an industrial chain integration among the metallurgical, cement, and chemical sectors, demonstrating the potential of H_2-driven Portland clinker production toward net-zero emissions targets. The innovations and advantages of this study are summarized as follows:

(*i*) Process innovation: This study proposes a novel process that integrates carbonate reduction calcination with methanol synthesis, enabling simultaneous source-level CO_2 emission reduction in cement production and effective utilization of industrial by-product gases. Unlike existing decarbonization process that focus on raw material and fuel substitutions or end-of-pipe CCUS deployment, the proposed scheme emphasizes process integration and resource synergy, thereby establishing a distinct and innovative process configuration.
(*ii*) Energy efficiency and deep decarbonization advantages: The proposed scheme demonstrates superior conprehensive performance in terms of energy efficiency and CO_2 emission reduction potential. In particular, the COG-driven configuration exhibits superior energy efficiency under industrial operating conditions, while the H_2-driven configuration achieves the lowest CO_2 emission intensity among the process routes considered in this study, thereby supporting deep decarbonization of the cement industry.
(*iii*) A detailed system-level assessment: A comprehensive evaluation framework combining process simulation, energy integration, techno-economic analysis, and CO_2 emission quantification has been employed to systematically assess the proposed scheme. The results are further compared with representative decarbonization strategies reported in the literature, thereby enhancing the analytical robustness and clarifying its position within the broader research landscape.
(*iv*) Industrial symbiosis potential: This study highlights the potential for cross-sectoral collaborative decarbonization, particularly in regions characterized by steel-cement industrial coupling. In such contexts, CO_2 generated from cement production can be partially utilized for the synthesis of methanol and other chemicals, facilitating industrial value chain upgrading.

2. Process description and modeling

2.1. Process description

As illustrated in Fig. 1, the proposed hydrogen-driven co-production of Portland clinker precursor and methanol consists of five subsystems: (*i*) Portland clinker precursor manufacture, (*ii*) pressure swing adsorption, (*iii*) methanol synthesis, (*iv*) heat pump distillation, and (*v*) gas-steam combined cycle. Firstly, the raw meal undergoes reduction calcination in the fluidized bed calciner to produce Portland clinker precursor, using COG sourced from a steel mill or pure H_2 generated from wind–photovoltaic coupled water electrolysis. The crude syngas generated from fluidized bed calciner outlet is subjected to gradient cooling and dehydration, followed by H/C ratio adjustment *via* pressure swing adsorption to meet the stoichiometric requirements, which subsequently serves as feedstock for methanol synthesis. Lastly, the crude methanol is purified *via* heat pump distillation, while the off gas and high-grade waste heat recovered from other subsystems are introduced

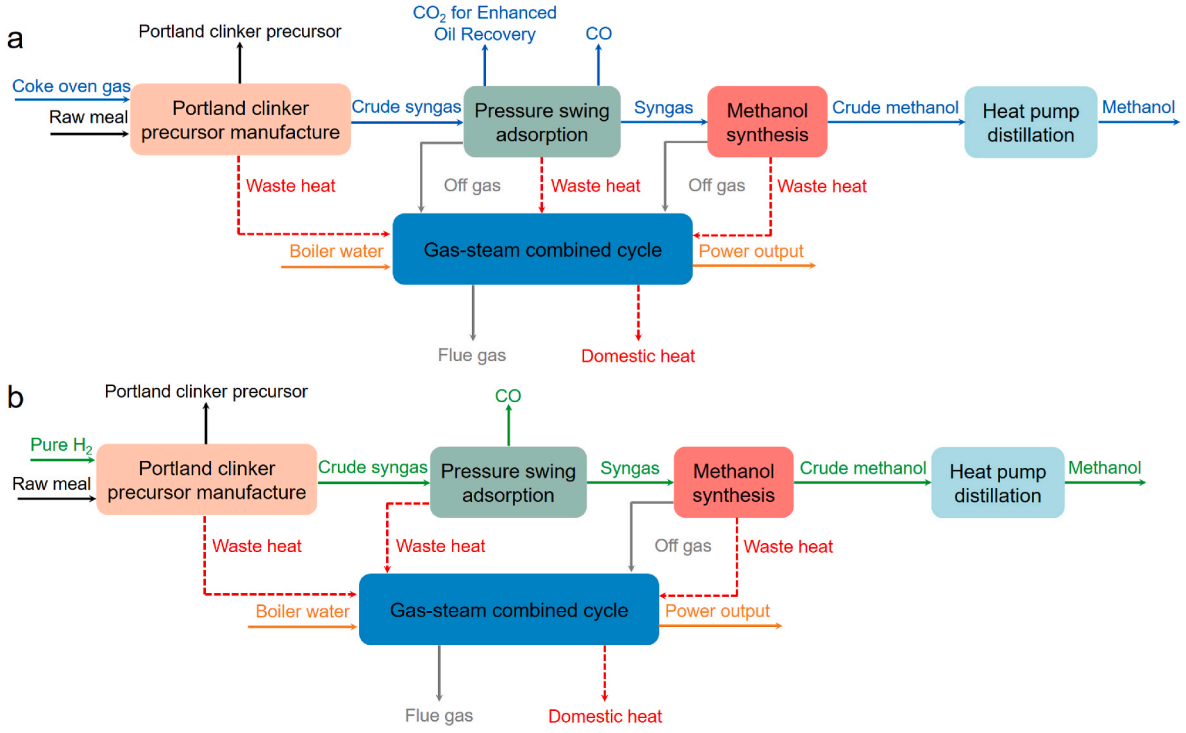

Fig. 1. Schematic of the hydrogen-driven co-production of Portland clinker precursor and methanol, with two scenarios for the hydrogen source: (a) coke oven gas and (b) pure H_2.

into the gas-steam combined cycle, achieving co-generation of heat and power.

2.2. Process modeling

The proposed process in Fig. 1 is simulated using Aspen Plus Version 11.0. The thermodynamic properties and binary interaction parameters are determined *via* Peng-Robinson equation of state (EOS) (Peng and Robinson, 1976), which is widely employed to describe multicomponent systems consisting of non-polar or weakly polar small gaseous molecules under high-temperature and moderate-to-low-pressure conditions. This EOS has been extensively applied in the thermodynamic analysis and modeling of high-temperature industrial processes, such as $CaCO_3$ decomposition and fuel gas reforming (Haaf et al., 2020; Hu and Ahn, 2017; Magli et al., 2022; Romano, 2013). In the carbonate reductive calcination considered in this study, the gas phase consists primarily of light species, including H_2, CO, CO_2, CH_4, N_2, and minor amounts of H_2O (g), all of which fall well within the applicable range of this EOS. The key

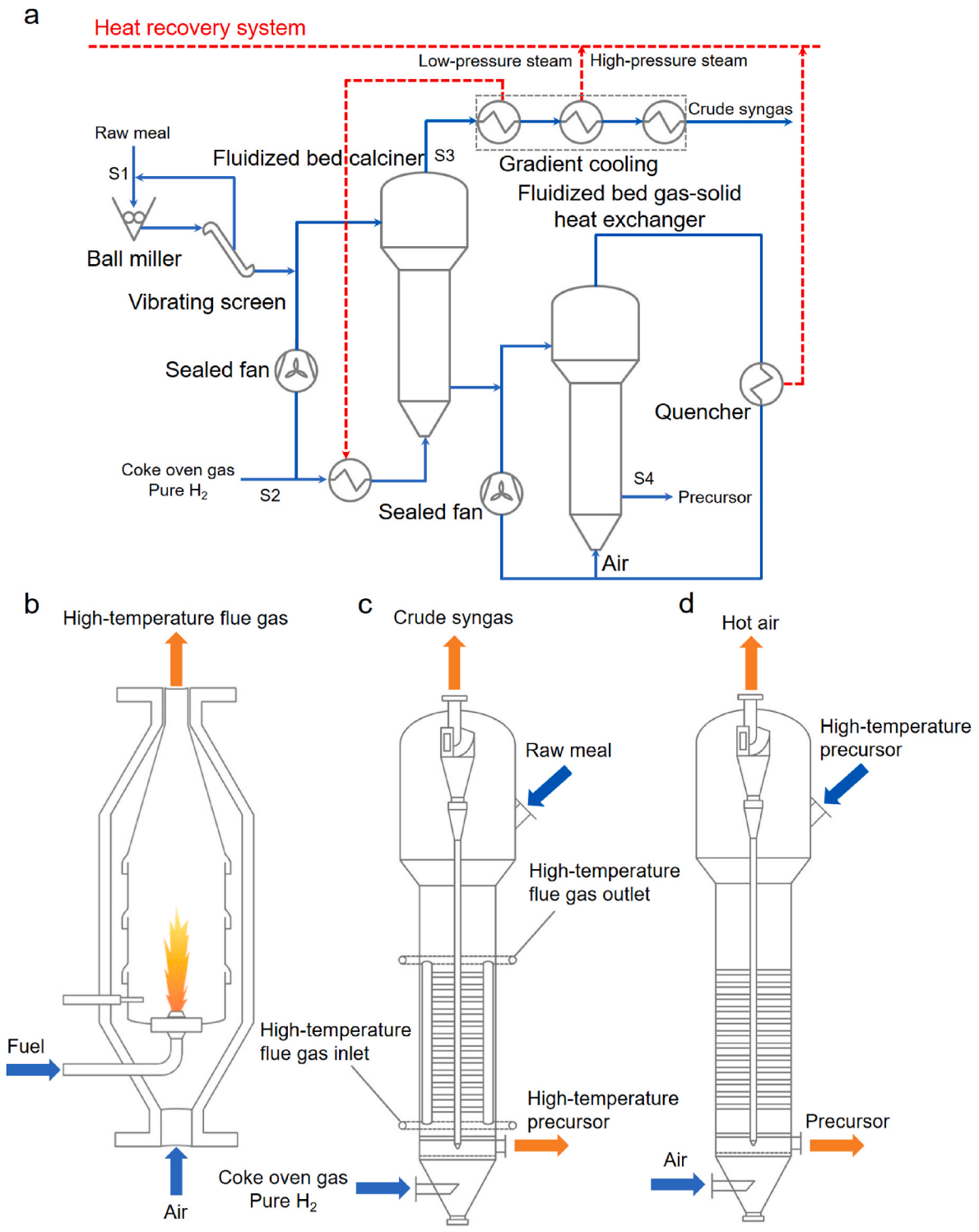

Fig. 2. Schematic of the Portland clinker precursor manufacture: (a) overall process flow diagram, (b) combustor, (c) fluidized bed calciner, and (d) fluidized bed gas-solid heat exchanger.

operating parameters of the respective unit are listed in Table S2 (ESI†).

2.2.1. Portland clinker precursor manufacture

As illustrated in Fig. 2(a), the raw meal is first ground in a ball miller, followed by classification of fine particles (≤200 μm) *via* a vibrating screen. Pneumatic conveying, employing COG or pure H_2 as the carrier gas, transports the raw meal to the fluidized bed calciner (equipped with a cyclone, Fig. 2(c)). High-temperature flue gas generated from complete fuel combustion in the combustor (Fig. 2(b)) supplies the heat required for carbonate reduction calcination. The crude syngas generated from the top of calciner undergoes gradient cooling before entering pressure swing adsorption, while the high-temperature Portland clinker precursor discharged from the bottom of calciner is introduced into fluidized bed gas-solid heat exchanger (Fig. 2(d)) to exchange heat with air and then is transferred to subsequent processes. In this subsystem, $CaCO_3$ undergoes reduction calcination at high temperatures: 950 °C when COG is employed as the hydrogen source and 700 °C for pure H_2. Under these operating conditions, $CaCO_3$ is completely decomposed, and the reaction system provides sufficient thermodynamic driving force such that $CaCO_3$ decomposition and gas-phase reforming are not limited by reaction kinetics. Therefore, adopting a thermodynamic equilibrium assumption to describe the reactant conversion in the calcination is justified (Nawaz and Ali, 2020; Wu et al., 2020). Table S3 (ESI†) represents the chemical reactions and conversions of reactants involved in Portland clinker precursor manufacture employing COG or pure H_2 as the hydrogen source, with corresponding descriptions of each module provided in Table S4 (ESI†). Additionally, the following assumptions are considered in this subsystem:

(*i*) The Portland clinker manufacture can be divided into five sequential stages: moisture evaporation (100–150 °C), clay dehydration (450 °C), carbonate decomposition (600–900 °C), solid-state mineral recombination (800–1300 °C), and clinkering phase formation (1300–1450 °C). Considering the constrained crystallization kinetics of clinker in the fluidized bed calciner, this study focuses primarily on carbonate decomposition, dry reforming of methane, and reverse water-gas shift.
(*ii*) The Portland clinker precursor typically consists of 63–68 wt% CaO, 20–24 wt% SiO_2, 4.0–9.5 wt% Al_2O_3, and <5 wt% MgO + Fe_2O_3 (Taylor, 1997).

Table 1 presents a comparison between simulation data and experimental data of Portland clinker precursor manufacture in the H_2-driven configuration. The simulated mass fractions of the major components in Portland clinker precursor, including CaO, SiO_2, Al_2O_3, and MgO + Fe_2O_3, show good agreement with the reported experimental ranges, with relative errors remaining within acceptable limits. In addition, the simulated CO selectivity of the crude syngas is consistent with the literature value, further supporting the reliability of the modeling for the H_2-driven configuration. It should be noted that, for the COG-driven configuration, direct validation against experimental or pilot-scale data is currently not available due to the lack of available measurements. Consequently, the COG-driven configuration is evaluated only at the level of thermodynamic analysis and process simulation.

Table 1
The experimental (Yu et al., 2025) and simulation data of Portland clinker precursor manufacture in the H_2-driven configuration.

Portland clinker precursor	Simulation data (wt.%)	Literature data (wt.%)	Relative error
CaO	65.09	66-67	−0.021
SiO_2	23.92	20-24	0.087
Al_2O_3	8.65	4-7	0.573
MgO + Fe_2O_3	2.35	2.5-6	−0.447
Crude syngas	Simulation data (%)	Literature data (%)	Relative error
CO selectivity	96.39	95.95	0.005
CO_2 selectivity	3.61	4.05	−0.109

2.2.2. Pressure swing adsorption

The crude syngas outlet from the calciner is introduced into pressure swing adsorption to adjust the H/C ratio required for methanol synthesis. Initially, for the COG-driven configuration, as shown in Fig. 3(a), the crude syngas is fed into gas-liquid separator to remove condensed water. In the first PSA unit, high purity H_2 (>99.999 vol%) is recovered. Regeneration of the adsorbent is achieved by depressurization, which is simulated by a valve located at the PSA bottom stream. The bottom stream is subsequently recompressed and cooled before entering the second PSA unit, where CO product (>99.5 vol%) is obtained from the top stream. The bottom stream of the second PSA unit is then fed into the third PSA unit for further purification. High purity CO_2 (>99.5 vol%) is recovered from the top stream, with a portion blended with H_2-rich and CO-rich streams as syngas. The residual off gas discharged from the bottom stream is routed to the gas-steam combined cycle. Similarly, for the H_2-driven configuration (Fig. 3(b)), the dehydrated crude syngas undergoes pressure swing adsorption to obtain high purity CO (>99.9 vol%). One portion is output as final CO product, while the remainder is blended with the desorbed components as syngas, which exhibits an H/C molar ratio of 0.17, necessitating external hydrogen supplementation for stoichiometric compensation. A typical PSA process is illustrated in Fig. 3(c). All units are modeled simplistically as ideal separators, operating under realistic conditions (35 °C, 30 bar). Notably, the syngas mainly consists of CO_2, CO, and H_2, whose mole fractions need to be adjusted to the optimal stoichiometric ratios (Eqs. (5)–(7)) (Puig-Gamero et al., 2018) to enhance methanol synthesis kinetics while simultaneously suppressing dimethyl ether formation through *in situ* water generation from CO_2 hydrogenation.

$$\frac{F_{H_2}\text{-}F_{CO_2}}{F_{CO}+F_{CO_2}} \approx 2.1 \tag{5}$$

$$\frac{F_{H_2}}{F_{CO}} = 2.4 - 2.5 \tag{6}$$

$$\frac{F_{CO_2}}{F_{CO}} = 0.13 - 0.14 \tag{7}$$

13X zeolite (Park et al., 2016) is selected as the adsorbent for pressure swing adsorption due to its commercial availability and proven effectiveness in industrial gas purification. The loading amount of 13X zeolite is determined by Eq. (8) (Yuan, 2019).

$$m_{total} = \sum_{i}^{n} \frac{q_{feed,i} \times \tau_i}{n_i} \tag{8}$$

where m_{total} (tonne) represents the loading amount of 13X zeolite; $q_{feed,\,i}$ (kmol/s) is the feed flow rate of the ith PSA unit; τ_i (s) denotes the adsorption time of the ith PSA unit; and n_i (kmol/tonne) is the adsorption capacity of adsorbed component. The adsorption capacities of H_2, CO, and CO_2 on 13X zeolite are 0.179 kmol/tonne, 2.300 kmol/tonne, and 5.422 kmol/tonne (Park et al., 2016), respectively. When COG is used as the hydrogen source, the adsorption time of the first PSA unit is set to 420 s (Gubin et al., 2025). For other scenarios, adsorption time is adjusted proportionally according to the respective feed flow rates. Detailed information on the percentage of component recovery and descriptions of each module in pressure swing adsorption are provided in Table S5 (ESI†) and Table S6 (ESI†), respectively.

2.2.3. Methanol synthesis

Upon achieving the target composition and purity, the syngas is subsequently fed into methanol synthesis. The descriptions of each module in methanol synthesis are detailed in Table S7 (ESI†) and the

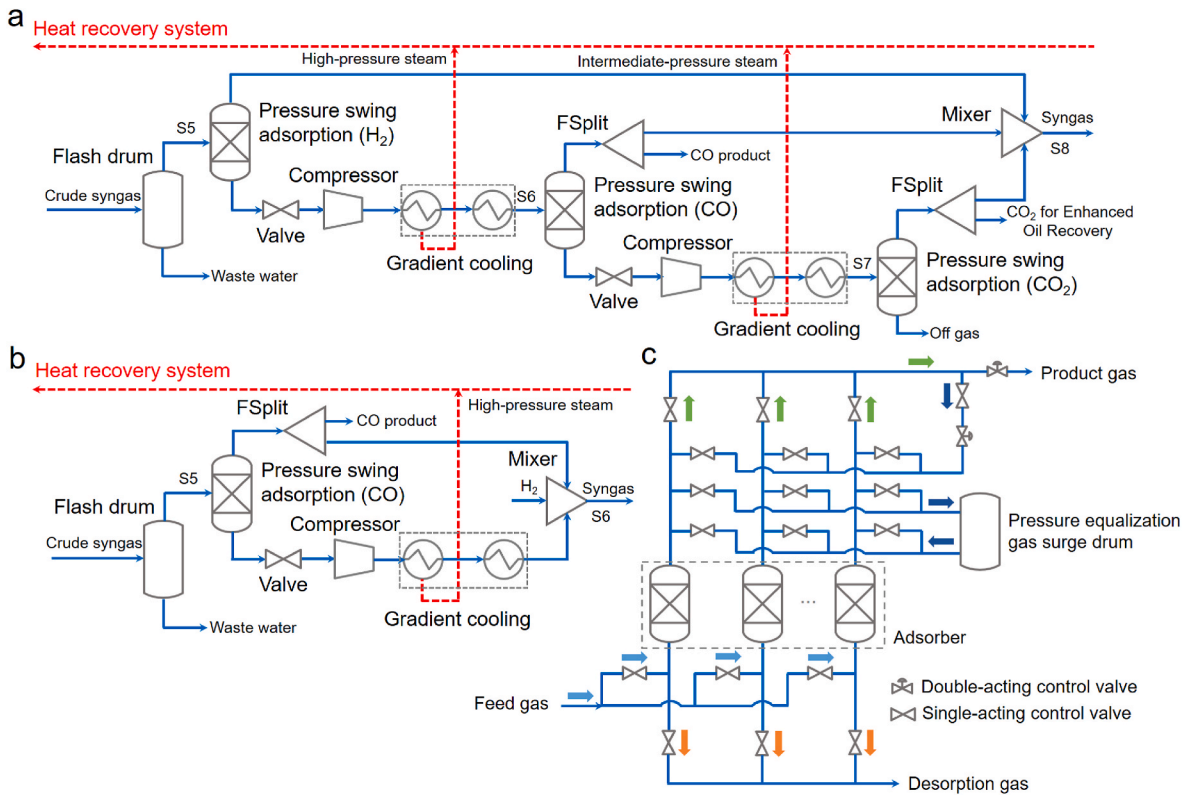

Fig. 3. Schematic of the pressure swing adsorption, showing two configurations for employing (a) coke oven gas and (b) pure H_2, respectively, accompanied by (c) a generic illustration of a typical pressure swing adsorption process.

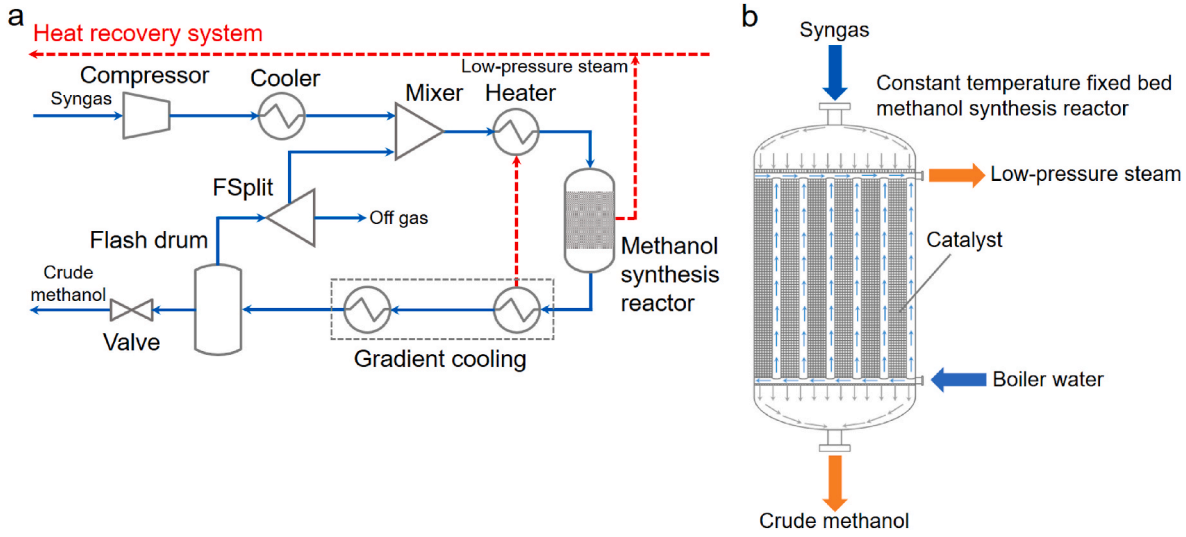

Fig. 4. Schematic of the methanol synthesis: (a) overall process flow diagram and (b) the corresponding methanol synthesis reactor.

overall process flowsheet is illustrated in Fig. 4(a). Firstly, the purified syngas is compressed and preheated to the specified operating pressure and temperature. It then enters the methanol synthesis reactor (Fig. 4 (b)) to accomplish methanol production. The required catalyst loading amount is calculated by:

$$m_{cat} = \frac{\pi}{4} d^2 \times l \times n \times (1\text{-}\varepsilon) \times \rho_{cat} \quad (9)$$

where m_{cat} (kg) denotes the loading amount of catalyst; d (m) is the tube diameter; l (m) is the tube length; n is the number of tubes; ε represents the catalyst bed voidage; and ρ_{cat} (kg/m^3) is the catalyst packing density.

The shell side of the tube bundles is filled with boiler water to recover the exothermic heat *via* low-pressure (LP) steam generation. The following reactions are involved during methanol synthesis (Kiss et al., 2016):

$$A)\ CO + 2H_2 \rightarrow CH_3OH\ \Delta H_{298K} = -90.77\ kJ/mol \quad (10)$$

$$B)\ CO_2 + H_2 \rightarrow CO + H_2O\ \Delta H_{298K} = +41.21 kJ/mol \quad (11)$$

$$C)\ CO_2 + 3H_2 \rightarrow CH_3OH + H_2O\ \Delta H_{298K} = -49.16\ kJ/mol \quad (12)$$

Notably, the reverse water-gas shift (Eq. (11)) is endothermic, hence

elevated temperature is thermodynamically favorable. In contrast, the hydrogenation of CO and CO_2 to methanol (Eqs. (10) and (12)) is exothermic, hence elevated temperature is thermodynamically unfavorable. Consequently, lower reaction temperature is preferred to enhance methanol yield, suppress CO byproduct formation, and mitigate catalyst sintering. The kinetics are based on Graaf's kinetic model of methanol synthesis, as shown in Eqs. (13)–(15) (Kiss et al., 2016). The corresponding kinetic parameters are summarized in Tables S8–S11 (ESI†).

$$r_{CH_3OH} = k_A \frac{K_{CO}\left(f_{CO} f_{H_2}^{1.5} \frac{f_{CH_3OH}}{K_A f_{H_2}^{0.5}}\right)}{\left(1 + K_{CO} f_{CO} + K_{CO_2} f_{CO_2}\right)\left(f_{H_2}^{0.5} + \frac{K_{H_2O} f_{H_2O}}{K_H^{0.5}}\right)} \tag{13}$$

$$r_{CO} = k_B \frac{K_{CO_2}\left(f_{CO_2} f_{H_2} \frac{f_{H_2O} f_{CO}}{K_B}\right)}{\left(1 + K_{CO} f_{CO} + K_{CO_2} f_{CO_2}\right)\left(f_{H_2}^{0.5} + \frac{K_{H_2O} f_{H_2O}}{K_H^{0.5}}\right)} \tag{14}$$

$$r_{CH_3OH} = k_C \frac{K_{CO_2}\left(f_{CO_2} f_{H_2}^{1.5} \frac{f_{H_2O} f_{CH_3OH}}{f_{H_2}^{1.5} K_C}\right)}{\left(1 + K_{CO} f_{CO} + K_{CO_2} f_{CO_2}\right)\left(f_{H_2}^{0.5} + \frac{K_{H_2O} f_{H_2O}}{K_H^{0.5}}\right)} \tag{15}$$

Due to chemical equilibrium limitations, the conversion is incomplete so the reactor outlet consists of products (CH_3OH and H_2O) as well as unconverted reactants (CO_x and H_2). The gas-phase mixture is subsequently cooled and subjected to the gas-liquid separator to remove the condensable components from the non-condensable gas. The mixture of CH_3OH-H_2O is further purified by heat pump distillation. The non-condensable gas is partially recycled to the methanol synthesis reactor, with the remainder sent to gas-steam combined cycle. The recycle stream determines overall methanol yield and reactor cooling duty. Enhancing atom economy requires a higher recycle fraction, thereby reducing the water content in crude methanol and boosting LP steam generation.

2.2.4. Heat pump distillation

Heat pump distillation, as an energy-efficient process intensification technology, is able to reduce the energy consumption by upgrading low-grade heat from the condenser to drive the reboiler (Díez et al., 2009; Kiss et al., 2012). As shown in Fig. 5, in this subsystem, crude methanol, after depressurization, is purified *via* overhead vapor direct-compression heat pump distillation. The top vapor from the distillation column is compressed to elevate its temperature and promote its energy to be more available. Then the high-temperature vapor subsequently provides the necessary heat to the reboiler *via* condensation-mediated heat exchange, facilitating the vaporization of the bottom column outlet stream. The vapor requires additional cooling before being recycled to the column, which is then divided into two fractions: one serves as the final CH_3OH product (>99.9 wt%), while the other is returned to the column. The bottom column outlet stream is fed into the flash drum, where the vapor phase is recycled back to the column, and the liquid phase is discharged as methanol-lean waste water. The descriptions of each module in heat pump distillation are provided in Table S12 (ESI†).

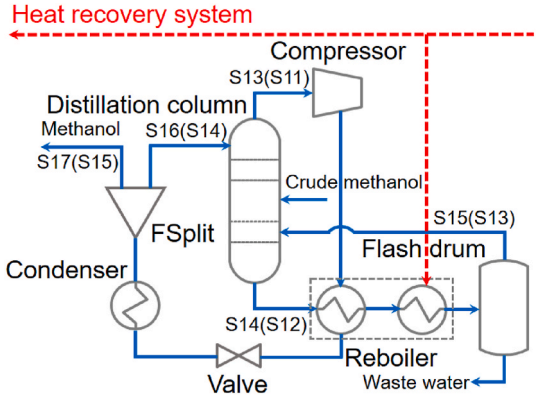

Fig. 5. Schematic of the heat pump distillation.

2.2.5. Gas-steam combined cycle

Achieving higher thermal efficiency is thermodynamically unattainable in standalone gas turbine or steam turbine (Kawabata et al., 2013). To overcome the limitation, this study adopts gas-steam combined cycle, wherein the exhaust heat from the gas turbine drives steam generation *via* heat recovery steam generator (HRSG), thereby enabling energy cascade utilization through sequential power generation. As illustrated in Fig. 6, the off gas mixed with air is combusted in the combustor, and the resulting high-temperature flue gas is transferred to the expansion turbine for power generation. The flue gas exiting the expansion turbine, together with residual heat from other subsystems, is recovered in serval HRSGs to generate steam. Along its width, the HRSG is equally divided into three functional zones: economizer, evaporator, and superheater. The generated steam, with respective state parameters detailed in Table S13 (ESI†), is directed to the steam turbine for additional power generation. The exhaust steam discharged from steam turbine outlet undergoes condensation, cooling, deaeration, and pressurization before being returned to the feedwater inlet of HRSG, establishing a closed-loop boiler water cycle. The descriptions of each module in gas-steam combined cycle are provided in Table S14 (ESI†).

2.3. Assessment criteria

2.3.1. Technical assessment

The technical feasibility indicators primarily include carbon utilization efficiency, overall energy efficiency, levelized energy consumption of Portland clinker precursor (LECOP, GJ per tonne), and levelized CO_2 emission of Portland clinker precursor (LCEOP, tonne CO_2 per tonne).

2.3.1.1. Carbon utilization efficiency. The carbon utilization efficiency (f) is defined as the ratio of the molar flow of carbon in the product stream ($F_{C,\ product}$, kmol/h) to that in the feedstock stream ($F_{C,\ feedstock}$, kmol/h), as shown in Eq. (16).

$$f = \frac{F_{C,product}}{F_{C,feedstock}} \times 100\% \tag{16}$$

2.3.1.2. Overall energy efficiency. The overall energy efficiency ($\eta_{overall}$) is defined as the ratio of energy output (E_{out}, MJ/h) to energy input (E_{in}, MJ/h), as shown in Eq. (17).

$$\eta_{overall} = \frac{E_{out}}{E_{in}} = \frac{n_{product} \times LHV_{product} + P_{electricity,out}}{n_{feedstock} \times LHV_{feedstock} + P_{electricity,in}} \times 100\% \tag{17}$$

where $n_{product}$ (kmol/h) and $n_{feedstock}$ (kmol/h) represent the molar flow of the product and feedstock, respectively; $LHV_{product}$ (MJ/kmol) and $LHV_{feedstock}$ (MJ/kmol) denote the low heating value (LHV) of the product and feedstock; $P_{electricity,\ out}$ (MW) and $P_{electricity,\ in}$ (MW) refer to the electricity output and electricity input, respectively. The LHVs of all components involved in the proposed process are listed in Table S15 (ESI†).

2.3.1.3. Levelized energy consumption of Portland clinker precursor. The LECOP is defined as the ratio of energy input to the total Portland clinker precursor output ($m_{precursor}$, tonne/h), as shown in Eq. (18).

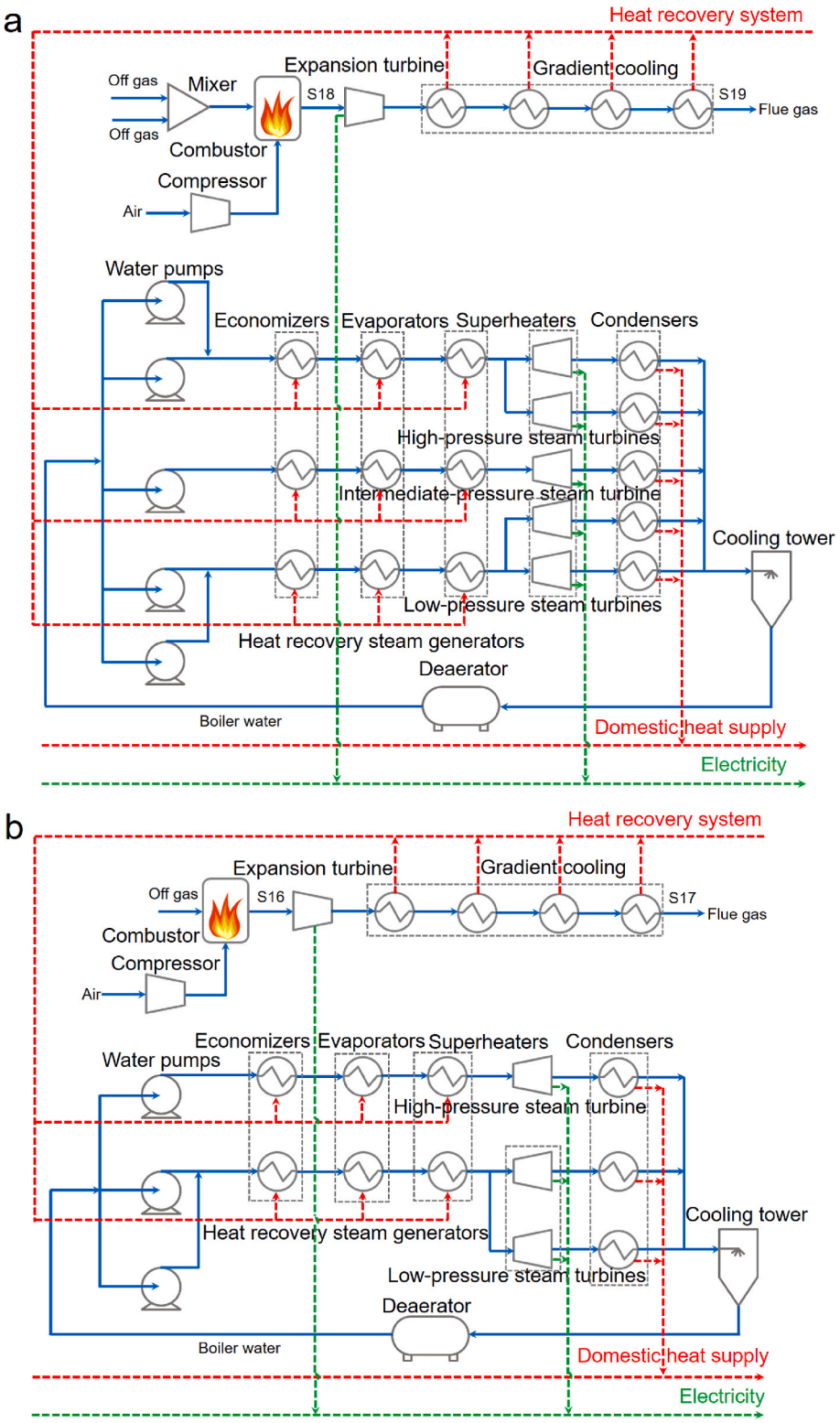

Fig. 6. Schematic of the gas-steam combined cycle under two hydrogen source configurations: (a) coke oven gas and (b) pure H_2.

$$LECOP = \frac{E_{in}}{m_{precursor}} \tag{18}$$

2.3.1.4. Levelized CO_2 emission of Portland clinker precursor. The LCEOP encompasses both direct and indirect emissions: direct emissions refer to CO_2 released from process outlet streams (excluding products), while indirect emissions arise from fuel and utility consumption (Zhang et al., 2024a, 2024b), as shown in Eq. (19).

$$LCEOP = \frac{m_{CO_2}^{direct} + \Sigma G_i \times C_i \times \alpha}{m_{precursor}} \tag{19}$$

where $m$direct CO_2(tonne/h) denotes direct CO_2 emissions; G_i (i.e., tonne/h) represents fuel and utility consumptions; C_i (i.e., kg coal equivalent (ce) per tonne) is the equivalent factors of standard coal

corresponding to various energy sources; and α (kg CO_2 per kg ce)is the carbon emission factor of standard coal (Table S16, ESI†).

In this study, steel production is defined as the upstream process, whereas the reduction calcination of cement raw meal is treated as the downstream process. COG is regarded as an inevitable by-product generated during steel production, and all process-related CO_2 emissions associated with its generation are entirely allocated to the primary steel product, without being further attribution to the downstream cement raw meal reduction calcination. In addition, the direct and indirect CO_2 emissions arising from the utilization of COG in the cement raw meal reduction calcination process are explicitly included within the system boundary. For the H_2-driven configuration, the upstream CO_2 emissions from hydrogen production are not directly included in the CO_2 emissions inventory of this study. Instead, they are internalized into the respective production costs *via* a carbon tax. This allocation strategy facilitates a clearer comparison of the environmental performance of alternative hydrogen sources during downstream utilization.

2.3.2. Economic assessment

Based on a bottom-up approach and a breakdown approach (ESI†), the total plant cost (TPC, million US dollars), total opex (TO, million US dollar per year), and total income (TI, million US dollar per year) can be estimated. The economic feasibility indicators, including annual profit (AP, million US dollars), net present value (NPV, million US dollars), internal rate of return (IRR, %), dynamic payback period (DPBP, years), levelized cost of Portland clinker precursor (LCOP, US dollar per tonne), and levelized profit of Portland clinker precursor (LPOP, US dollar per tonne) are defined to comprehensively assess the competitiveness of the proposed process. To account for temporal cost variations, including inflation, the Chemical Engineering Plant Cost Index (CEPCI) is employed to revise the cost functions, with 2023 selected as the base year.

The AP is employed to assess the profitability of the proposed process within a given year, defined as the difference between the TI and TO, as shown in Eq. (20).

$$AP = TI - TO \tag{20}$$

The NPV quantifies the present value of all expected net cash inflows generated by the proposed process throughout its entire lifecycle, discounted to a reference point using a specified baseline discount rate i_0, as shown in Eq. (21). The IRR is defined as the discount rate at which the NPV equals zero, as shown in Eq. (22), which is widely employed to assess the economic feasibility of the proposed process. If the IRR exceeds the baseline discount rate i_0, the investment is considered acceptable from an economic standpoint. Conversely, the proposed process is economically unfeasible and not worth investing in. Moreover, a higher IRR indicates stronger investment attractiveness and greater potential economic return.

$$NPV = \Sigma_{t=0}^{n} \frac{(TI\text{-}TO)_t}{(1+i_0)^t} \tag{21}$$

$$\Sigma_{t=0}^{n} \frac{(TI\text{-}TO)_t}{(1+IRR)^t} = 0 \tag{22}$$

Several assumptions related to the economic feasibility analysis are listed in Table S23 (ESI†). No revenue is generated during the first and second years, as the plant is under construction. Commercial operation begins in the third year with a production capacity of 60%, which ramps up to full capacity (100%) starting from the fourth year. The straight-line depreciation method is adopted to calculate depreciation expenses.

The DPBP is defined as the year in which the NPV turns zero for the first time, as shown in Eq. (23).

$$DPBP = T - 1 + \frac{\left|\Sigma_i^{T\text{-}1} \frac{(TI\text{-}TO)_i}{(1+i_0)^i}\right|}{\frac{(TI\text{-}TO)_T}{(1+i_0)^T}} \tag{23}$$

The LCOP and LPOP are defined as the allocations of the TO and AP over the total Portland clinker precursor output, expressed on a per-tonne basis. These metrics enable direct comparison of economic performance across different technological pathways or process configurations, as shown in Eqs. (24) and (25).

$$LCOP = \frac{TO}{m_{\text{precursor}}} \tag{24}$$

$$LPOP = \frac{AP}{m_{\text{precursor}}} \tag{25}$$

3. Results and discussion

3.1. Process simulation

The parameters of the key streams marked in Figs. 2–6 for the proposed hydrogen-driven co-production of Portland clinker precursor and methanol are listed in Tables S24 and S25 (ESI†), which serve as the foundation for subsequent energy integration and techno-economic analysis. Table 2 summarizes the energy input-output results of two process configurations, aiming to preliminarily reflect their practical applicability. Notably, at consistent output of Portland clinker precursor, for the COG-driven configuration, the heat duty of fluidized bed calciner (104.19 MW_{th}) is 60% higher than that of the H_2-driven configuration (65.16 MW_{th}), which originates from higher calcination temperature (950 °C vs 700 °C) and strongly endothermic characteristic of dry methane reforming. In contrast, the overall heat duty of the H_2-driven configuration (49.96 MW_{th}) is significantly lower than that of COG-driven configuration (137.75 MW_{th}), resulting in reduced power generation. Nevertheless, the COG-driven configuration exists a power gap of 1.6 MW (14.34 MW of total power output vs 15.94 MW of total power input), whereas the H_2-driven configuration exists a net power output of 3.44 MW (5.08 MW of total power output vs 1.64 MW of total power input), revealing its unique advantage of electricity self-sufficiency.

3.2. Techno-economic analysis

Table 3 summarizes the key techno-economic indicators for the proposed hydrogen-driven co-production of Portland clinker precursor and methanol. From a technical standpoint, the H_2-driven configuration achieves a carbon utilization efficiency of 99.74%, surpassing that of the COG-driven configuration (86.30%), and indicating near-complete carbon conversion. This advantage is clearly reflected in the direct CO_2 emissions, which decrease from 2.72 tonne/h in the COG-driven configuration to only 0.07 tonne/h in the H_2-driven configuration. Moreover, owing to lower fuel and utility consumption, the H_2-driven configuration exhibits reduced indirect CO_2 emissions, declining from

Table 2
Energy input-output results for the proposed hydrogen-driven co-production of Portland clinker precursor and methanol.

Item	Parameter	Coke oven gas	Pure H_2
Heat duty of fluidized bed calciner	$Q_{d,\ cal}$ (MW_{th})	104.19	65.16
Overall heat duty	Q_d (MW_{th})	137.75	49.96
Total cooling water consumption	Q_{cw} (tonne/h)	2084.25	612.37
Total boiler water consumption	Q_{bw} (tonne/h)	77.71	36.34
Power input of sealed fan	P_s (kW)	7.78	2.40
Total power input	P_{in} (MW)	15.94	1.64
Total power output	P_{out} (MW)	14.34	5.08

Table 3
Key techno-economic indicators for the proposed hydrogen-driven co-production of Portland clinker precursor and methanol.

Technical indicator	Coke oven gas	Pure H_2
Carbon utilization efficiency (%)	86.30	99.74
Direct CO_2 emissions (tonne/h)	2.72	0.07
Indirect CO_2 emissions (tonne/h)	32.82	18.93
Levelized CO_2 emission of Portland clinker precursor (LCEOP) (tonne CO_2 per tonne)	0.55	0.29
Overall energy efficiency (%)	63.57	58.79
Levelized energy consumption of Portland clinker precursor (LECOP) (GJ per tonne)	18.17	8.51
Economic indicator	**Coke oven gas**	**Pure H_2**
Total plant cost (TPC) (million US dollars)	550.25	230.61
Total opex (TO) (million US dollar per year)	100.39	143.51
Total income (TI) (million US dollar per year)	202.38	145.65
Annual profit (AP) (million US dollars)	101.99	2.14
Dynamic payback period (DPBP) (years)	11.84	N.A.
Internal rate of return (IRR) (%)	16.01	−13.73
Net present value (NPV) (million US dollars)	134.17	−199.71
Levelized cost of Portland clinker precursor (LCOP) (US dollar per tonne)	215.55	308.13
Levelized profit of Portland clinker precursor (LPOP) (US dollar per tonne)	218.98	4.59

32.82 to 18.93 tonne/h, which in turn results in a significantly lower LCEOP, from 0.55 to 0.29 tonne CO_2 per tonne. However, in terms of overall energy efficiency, the COG-driven configuration performs better, reaching 63.57% compared to 58.79% for the H_2-driven configuration. This improvement is primarily associated with the utilization of COG as the hydrogen source, which leads to a substantially higher LECOP (18.17 vs 8.51 GJ per tonne), due to the higher LHV of COG relative to pure H_2 (366.4 MJ/kmol vs 241.7 MJ/kmol). Despite the increased energy input, the CH_3OH output of the COG-driven configuration is 3.95 times higher than that of the H_2-driven configuration. Consequently, the energy output of the COG-driven configuration is 2.31 times greater, resulting in a significant enhancement in overall energy efficiency.

From an economic standpoint, the total plant cost (TPC) of the COG-driven configuration amounts to 550.25 million US dollars, which is approximately 2.39 times higher than that of the H_2-driven configuration (230.61 million US dollars). As illustrated in Fig. 7, for both COG and H_2-driven configurations, the owner's cost and contingency (OCC) and total equipment cost (TEC) represent the core components of the TPC, together accounting for more than 60%. It should be emphasized that, since the proposed processes remain at the conceptual design level with relatively low technology readiness level (TRL), a higher OCC has been applied, representing an additional key contributor to the TPC. In the COG-driven configuration, heat exchangers (including steam generators) and pressure swing adsorption are the major expenditure items, together contributing around 50% of the TEC. In contrast, for the H_2-driven configuration, the major equipment costs are associated with heat exchangers (including steam generators) and methanol synthesis reactor, which together constitute about 50% of the TEC (Fig. 8). As presented in Table 3, the total opex (TO) of the COG-driven configuration is 100.39 million US dollar per year, which is lower than that of the H_2-driven configuration, at 143.51 million US dollar per year. Among the various cost components, raw material costs as well as maintenance, insurance and taxes constitute the major shares. Notably, for the H_2-driven configuration, raw material costs alone account for up to 75% of the TO, primarily due to the high price of green H_2 (5.47 US dollar per kg) (Ahmadullah et al., 2025) and its limited supply capacity (1.84×10^4 tonne per year) (Fig. 9).

From a feasibility standpoint, the COG-driven configuration exhibits favorable economic performance, achieving an annual profit (AP) of 101.99 million US dollars, an internal rate of return (IRR) of 16.01%, a dynamic payback period (DPBP) of 11.84 years, a net present value (NPV) of 134.17 million US dollars, and a levelized profit of 218.98 US dollar per tonne Portland clinker precursor (Table 3). Conversely, under the considered production scales (Portland clinker precursor: 4.66×10^5 tonne per year, methanol: 5.37×10^4 tonne per year, CO: 3.38×10^6 m^3 per year) and market conditions (Portland clinker precursor: 111.4 US dollar per tonne (GTAIC, 2025), methanol: 0.412 euro per kg (Siskos et al., 2026), CO: 0.60 US dollar per kg (Mamun and Talukder, 2024)) in this study, the H_2-driven configuration is not economically feasible, failing to achieve investment recovery. Considering future trends, we anticipate that technology development should focus on large-scale, low-cost renewable energy-driven water electrolysis for green hydrogen production. It is expected to improve the economic viability of the H_2-driven configuration and enable deep decarbonization in carbonate-based material industry. In this study, the assumed prices of methanol and CO are derived from recently published literature, aiming

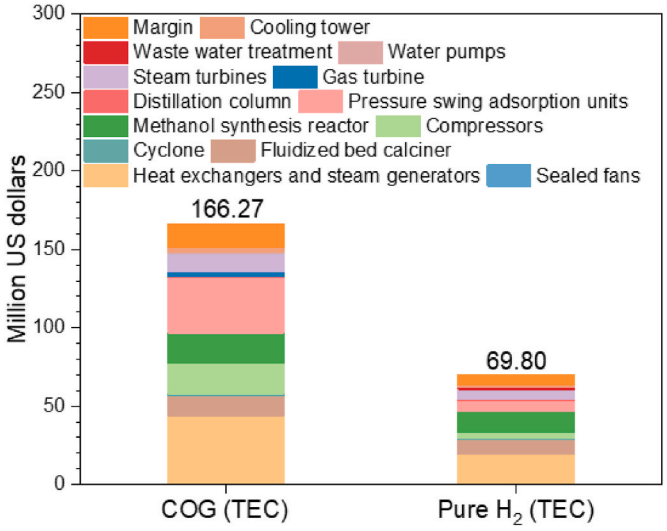

Fig. 8. Breakdowns of the total equipment cost (TEC) for the coke oven gas (COG) and pure H_2.

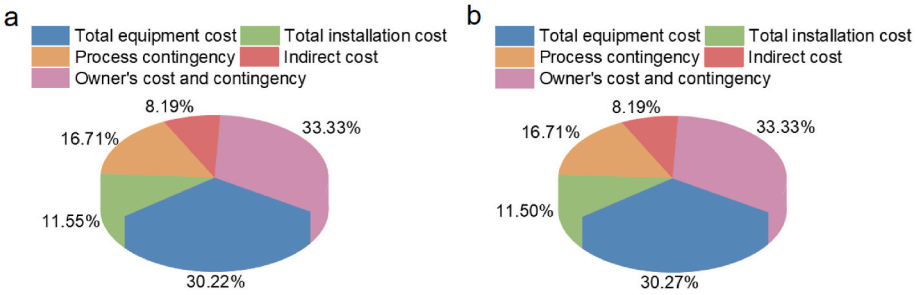

Fig. 7. Breakdowns of the total plant cost for the two hydrogen source scenarios: (a) coke oven gas and (b) pure H_2.

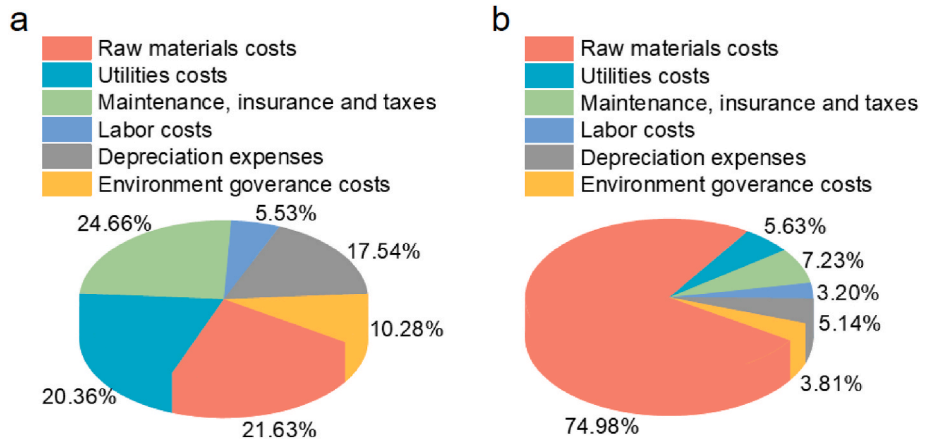

Fig. 9. Breakdowns of the total opex for the two hydrogen source scenarios: (a) coke oven gas and (b) pure H_2.

to reflect representative market price levels under current and short- to medium-term. Moreover, this study does not assume unlimited market absorption capacity for these by-product chemicals. Instead, methanol and CO are considered general-purpose chemical products with stable industrial demand. The economic performance of the proposed scheme is thus evaluated under reasonable and realistic production scales.

In 2022, China's coke production reached 473.44 million tonnes, with a by-product output of approximately 200 billion m^3 of COG. However, only 98.12 billion m^3 of COG were utilized (Di et al., 2024), indicating that there is a substantial surplus of COG for the most steel plants, fully meeting the requirements of the scenarios considered in this study (1.17×10^7 m^3 per year). The COG-driven configuration emerges as the more pragmatic and readily implementable solution in the short- to medium-term, thereby enabling synergistic decarbonization across the steel and cement industries, which is manifested in the following aspects:

(*i*) The steel and cement industries exhibit significant complementarities at the material and energy flow levels. By-products generated during steel production, including COG, blast furnace gas, and waste heat, have high energy quality and reuse potential. Meanwhile, the cement raw meal reduction calcination requires continuous high-temperature heat sources and reducing gases. The coupling of the steel and cement industries, along with facility co-location, enables the on-site utilization of these by-products, thereby enhancing primary energy efficiency in steel production and reducing the CO_2 emission intensity of steel.
(*ii*) The low-carbon transition pathways and temporal scales of the steel and cement industries are not fully synchronized. Although the steel industry is gradually shifting towards low-carbon processes, such as hydrogen-based direct reduction and electric arc furnace steelmaking, the cement industry, in the short- to medium-term, remains reliant on the high-temperature calcination of carbonates. During its transitional period, promoting industry coupling and facility co-location can facilitate the effective utilization of by-products from steel production to support the cement industry's low-carbon development, thereby mitigating the efficiency losses associated with isolated decarbonization efforts within individual industries.
(*iii*) The steel and cement industries exhibit substantial potential for infrastructure synergies in energy supply, gas transportation, waste heat recovery, and environmental management. Through industry coupling and facility co-location, the need for additional pipeline construction can be minimized, thereby lowering operational costs in both industries and enhancing overall system efficiency.
(*iv*) The coupling of the steel and cement industries is consistent with current policy agendas that promote collaborative industrial CO_2 emission reduction and circular economy development. As a result, such initiatives are more likely to attract financial support, providing critical external conditions for the successful deployment of related projects. This strategy can not only enhance overall system efficiency and shorten the CO_2 reduction timeline, but also create favorable conditions for the subsequent shift to low carbon processes. The H_2-driven configuration represents a cornerstone technology for deep decarbonization. Its widespread application potential and economic viability are intrinsically linked to the rigor of governmental decarbonization policies, rendering it a particularly compelling alternative in regions endowed with abundant renewable resources and supported by ambitious legislative frameworks, such as Europe and the Middle East.

3.3. Sensitivity analysis

The proposed hydrogen-driven co-production of Portland clinker precursor and methanol is designed to achieve source-level CO_2 mitigation in the cement industry, while effectively mitigating the economic risks associated with volatilities in raw material and product market prices. To assess the economic robustness of the proposed process, a detailed sensitivity analysis of key factors influencing the economic performance is essential. In addition, considering the increasingly stringent domestic and international regulations on environmental protection and CO_2 emissions reduction, it is also imperative to evaluate the potential impact of carbon tax.

As illustrated in Fig. 10, the impacts of volatilities in product market prices and carbon tax on the AP, IRR, DPBP, LCOP, and LPOP in the COG-driven configuration are investigated. Notably, even under unfavorable market conditions—specifically, a 40% decrease in Portland clinker precursor price (to 66.84 US dollar per tonne), a 20% decrease in methanol price (to 0.330 euro per kg), and a 40% decrease in CO price (to 0.36 US dollar per kg)—the IRR remains above the baseline discount rate, indicating strong economic resilience to risks. However, when the carbon tax exceeds 120 US dollar per tonne CO_2, the IRR falls below the baseline discount rate, weakening profitability and suggesting that the carbon tax imposes a stringent constraint on the economic feasibility of the proposed process.

When the steel industry is gradually shifting toward low-carbon processes, such as hydrogen-based direct reduction and electric arc furnace steelmaking, the long-term availability of COG is likely to decline in parallel with reductions in coking capacity. At the process level, this trend may constrain the applicability of COG for the reductive calcination of cement raw meal. This phenomenon can be regarded as a potential "crowding-out effect" in cross-industry collaborative decarbonization, whereby the advancement of the steel industry's own decarbonization pathways inherently weakens its ability to supply by-product resources to the cement industry. Given the inherently

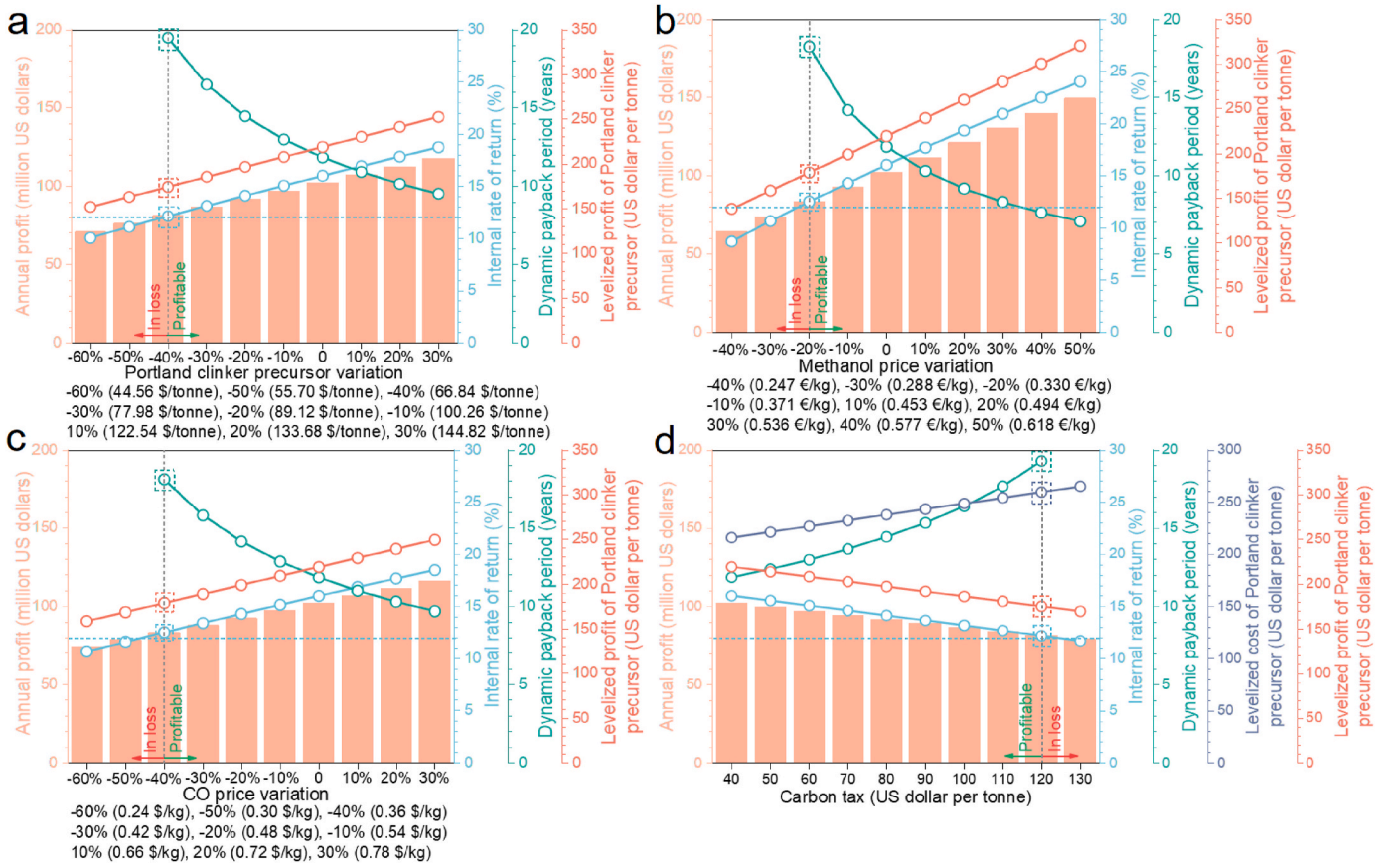

Fig. 10. Sensitivity analysis of key factors affecting the economic viability of the coke oven gas-driven configuration, evaluating the influence of: (a) Portland clinker precursor price, (b) methanol price, (c) CO price, (d) carbon tax.

gradual and staged nature of the steel industry's low-carbon transition, this study explicitly positions COG as a transitional resource for cross-industry collaborative decarbonization rather than a long-term or ultimate solution, thereby avoiding technological path dependence on COG supply at the process level. Furthermore, once the steel industry completes its low-carbon transition and the availability of associated by-product resources declines substantially. The deep decarbonization of cement industry will rely on alternative pathways, including the use of green H_2 as a calcination gas, the electrification of high-temperature processes, and the coordinated deployment of CCUS.

As illustrated in Fig. 11, if the prices of Portland clinker precursor, methanol, and CO increase by 70% (to 189.38 US dollar per tonne), 140% (to 0.989 euro per kg), and 50% (to 0.90 US dollar per kg), respectively, the IRR of the H_2-driven configuration exceeds the baseline discount rate. It indicates that, in the absence of corresponding policy subsidies, the economic feasibility of the H_2-driven configuration is highly dependent on favorable (albeit potentially artificial) price scenarios. If pure H_2 is generated from steam methane reforming coupled with CO_2 capture, with a hydrogen price of 1.4 US dollar per kg H_2 (Detz et al., 2018), the IRR of H_2-driven configuration can reach 29.27%, significantly surpassing the baseline discount rate. However, its economic viability is closely tied to the fossil fuel-based hydrogen supply chain. Alternatively, when pure H_2 is sourced from supercritical water gasification of soybean straw, with a hydrogen price of 1.94 US dollar per kg H_2 (Okolie et al., 2021), the AP of H_2-driven configuration can reach 67.17 million US dollars, with a dynamic payback period of 6.60 years, which demonstrates that employing green hydrogen derived from selective biomass gasification (Okolie et al., 2021; Wu et al., 2023) can make the proposed process economically advantageous, thereby offering a sustainable strategy that simultaneously ensures CO_2 emissions reduction and economic feasibility. Furthermore, If the cost of green H_2 generated from wind–photovoltaic coupled water electrolysis falls below 3.74 US dollar per kg and is available for large-scale supply, the green H_2-driven configuration will demonstrate both economic feasibility and environmental sustainability.

Table 4 provides a comparison of CO_2 emission intensities between the proposed processes and representative cement decarbonization pathways reported in the literature. The conventional route exhibits the highest CO_2 emissions, reaching 0.88 tonne CO_2 per tonne clinker. By contrast, mitigation measures such as raw material substitution and hydrogen-based fuel substitution reduce CO_2 emissions to 0.57 and 0.56 tonne CO_2 per tonne clinker, respectively, whereas improvements in energy efficiency alone yield only a limited reduction, with CO_2 emissions remaining at 0.85 tonne CO_2 per tonne clinker. The deployment of end-of-pipe CCUS achieves a more substantial reduction, lowering CO_2 emissions to 0.44 tonne CO_2 per tonne clinker. Against this backdrop, the proposed processes in this study demonstrate competitive and superior CO_2 mitigation potential. Specifically, the COG-driven configuration attains a CO_2 emission intensity of 0.55 tonne CO_2 per tonne clinker, comparable to that of hydrogen-based fuel substitution. In contrast, the H_2-driven configuration delivers the lowest CO_2 emissions among all considered routes, at 0.29 tonne CO_2 per tonne clinker. These results highlight the substantial CO_2 mitigation potential of the H_2-driven configuration, which enables deep decarbonization in the cement industry.

It should be further noted that, the present analysis is based on steady-state simulations and does not account for dynamic operational fluctuations and load variations associated with long-term industrial operation. These simplifying assumptions may introduce some uncertainties in the estimation of process-level operating costs and the identification of optimal operational strategies. However, they are unlikely to fundamentally affect the conclusions from the comparative

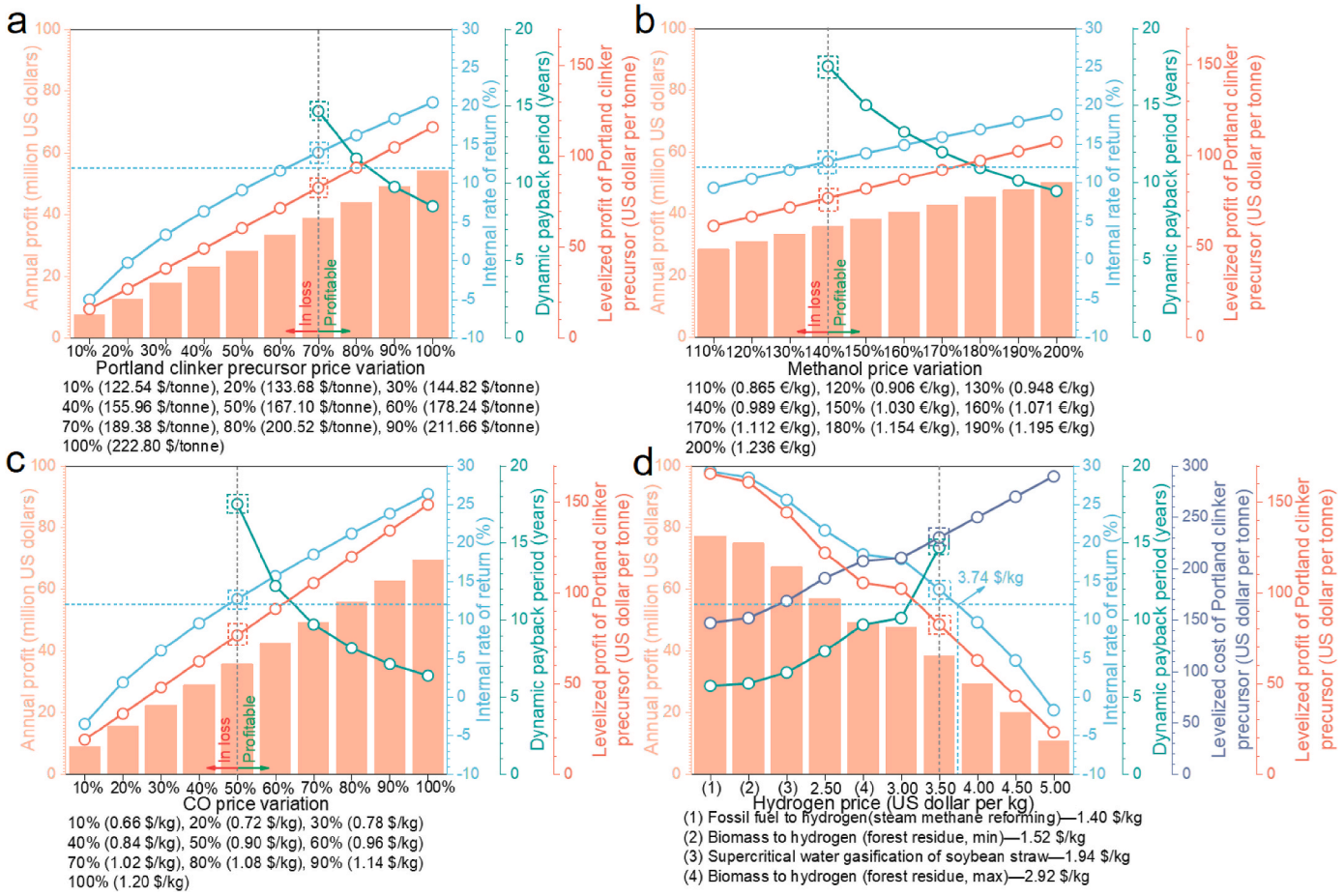

Fig. 11. Sensitivity analysis of key factors affecting the economic viability of the pure H_2-driven configuration, evaluating the influence of: (a) Portland clinker precursor price, (b) methanol price, (c) CO price, and (d) hydrogen price.

Table 4
Comparison of CO_2 emissions between the proposed processes and representative cement decarbonization pathways.

Route	CO_2 emissions (tonne CO_2 per tonne clinker)	Reference
Traditional process	0.88	Hills et al. (2016)
Raw material substitution	0.57	Williams and Yang (2024)
Fuel substitution (H_2)	0.56	Williams et al. (2024)
Energy efficiency enhancement	0.85	Pardo et al. (2011)
End-of-pipe carbon capture, utilization and storage (CCUS) deployment	0.44	Buli (2025)
Coke oven gas-driven configuration	0.55	This work
Pure H_2-driven configuration	0.29	This work

analysis of the different process configurations considered in this study. From an industrial-scale perspective, cement production typically operates at capacities on the order of tens of millions of tonnes per year, whereas methanol production is generally conducted at the million-tonne scale. This substantial mismatch in production scale implies that CO_2 generated during cement production cannot be fully utilized for methanol synthesis at the industry level, thereby potentially constraining large-scale implementation. Nevertheless, this issue mainly pertains to engineering design and system integration considerations, rather than compromising the technical feasibility and the CO_2 emission reduction potential of the proposed scheme. Accordingly, the proposed scheme is not intended for universal application across all cement plants, but rather targets specific industrial scenarios in which the steel and cement industries are co-located, serving as a regional pathway for cross-industry collaborative decarbonization. In this context, the associated by-products are more suitably consumed within coupled steel-cement industrial parks rather than being marketed as standalone bulk commodities for long-distance transport. Therefore, although the assumed production scales are technically feasible at the process level, their practical implementation and economic performance remain dependent, to some extent, on regional industrial structures and downstream absorption capacity.

From a technology maturity perspective, the proposed processes are currently positioned at an early development stage (Technology Readiness Level: 3-4), as existing evidence is primarily based on process simulation results and limited experimental studies reported in the literature. With respect to reactor durability, carbonate reductive calcination and similar high-temperature gas-solid reactions are typically implemented in industrial practice using rotary kilns (Hou et al., 2020; Ma et al., 2024; Xu et al., 2025), which are generally lined with refractory materials and enclosed by an outer shell fabricated from high-temperature-resistant alloy steel. Under this structural configuration, the reactive gas is effectively isolated from the metallic shell by the dense refractory lining, whose permeability is negligible at the engineering scale. As a result, potential gas leakage risks are mainly associated with the kiln inlet, outlet, and interface sections, rather than the

reactor body itself, and can be effectively mitigated through well-established sealing designs. For example, the CO_2GRAB/HYIRON project in Germany has constructed and commissioned a hydrogen-based, gas-tight rotary kiln pilot facility in the Emsland region, where green direct reduced iron is produced using H_2 as the reducing gas in a purpose-designed sealed rotary kiln. This project demonstrates the engineering feasibility of operating rotary kilns under pure H_2 (HyIron, 2023). Key engineering issues, such as rotary kiln configuration optimization, heat supply strategies, and operational safety management, warrant further investigation in subsequent engineering design and demonstration stages. However, these uncertainties primarily influence considerations related to industrial deployment and technology scale-up, and do not fundamentally affect the CO_2 emission reduction potential identified at the theoretical and system-integration levels in this study.

4. Conclusions

To mitigate the high CO_2 emissions from cement manufacture, co-production of Portland clinker precursor and methanol driven by COG or pure H_2 is proposed and evaluated through a systematic techno-economic assessment. When driven by COG, the proposed process achieves a levelized CO_2 emission of 0.55 tonne CO_2 per tonne Portland clinker precursor and demonstrates superior economic performance, with a net present value of 134.17 million US dollars, an internal return rate of 16.01%, and a dynamic payback period of 11.84 years over its entire lifetime. The COG-driven configuration effectively mitigates the economic risks associated with volatilities in raw material and product market prices and enables industrial chain synergy among the steel, cement, and chemical industries, overcoming the bottleneck of increasing marginal costs of CO_2 emission reduction within individual industries and providing a technically scalable solution during the low-carbon transition. When the proposed process is driven by pure H_2 generated *via* steam methane reforming, it achieves a carbon utilization efficiency of 99.74%, a levelized energy consumption of 8.51 GJ per tonne Portland clinker precursor, and a levelized CO_2 emission of 0.29 tonne CO_2 per tonne Portland clinker precursor while remaining economically attractive. Notably, the use of green H_2 from selective biomass gasification or wind–photovoltaic coupled water electrolysis (price $<$3.74 US dollar per kg H_2) further highlights the potential for deep decarbonization under moderate cost increments. Overall, the proposed processes enable complementary utilization of carbon and hydrogen resources across industries, and provide a viable and scalable pathway for deep decarbonization of the traditional carbonate-based material industry.

CRediT authorship contribution statement

Dongliang Zhang: Writing – original draft, Visualization, Investigation, Formal analysis, Data curation. **Hanke Li:** Methodology. **Qiangqiang Wu:** Validation. **Xiangdong Yu:** Investigation, Data curation. **Hao-Fan Wang:** Supervision, Resources. **Yonghai Cao:** Supervision, Resources. **Hongjuan Wang:** Supervision, Resources. **Siyu Yang:** Writing – review & editing, Supervision, Software, Funding acquisition. **Hao Yu:** Writing – review & editing, Supervision, Resources, Project administration, Funding acquisition, Conceptualization.

AI declaration

The authors confirm that no content generated by AI tools was used to create this manuscript. Any AI-assisted tools were only used for minor language or formatting edits and did not affect the scientific content.

Declaration of competing interest

The authors declare the following financial interests/personal relationships which may be considered as potential competing interests: Hao Yu and Siyu Yang reports financial support was provided by Hao Yu, the Professor of Chemcial Engineering, South China University of Technology. If there are other authors, they declare that they have no known competing financial interests or personal relationships that could have appeared to influence the work reported in this paper.

Acknowledgements

This work was supported by the Joint Funds of the National Natural Science Foundation of China (No. U22A20415), the Natural Science Foundation of Guandong Province (No. 2024B1515040016) and Guizhou Provincial Science and Technology Plan Project Natural Science Key Project (ZK[2022] 028).

Appendix A. Supplementary data

Supplementary data to this article can be found online at https://doi.org/10.1016/j.jclepro.2026.147949.

List of abbreviations

Abbreviations	
AP	Annual profit
CCUS	Carbon capture, utilization and storage
CEPCI	Chemical Engineering Plant Cost Index
COG	Coke oven gas
CP	Compressor
CT	Cooling tower
DC	Distillation column
DPBP	Dynamic payback period
EC	Equipment cost
ECO	Economizer
EOR	Enhanced oil recovery
EPC	Engineering, procurement and construction cost
ET	Expansion turbine
EU	European Union
EVA	Evaporator
FB	Fluidized bed
FBC	Fluidized bed calciner
FO	Fixed opex
IRR	Internal rate of return
LCEOP	Levelized CO_2 emission of Portland clinker precursor
LCOP	Levelized cost of Portland clinker precursor
LECOP	Levelized energy consumption of Portland clinker precursor
LHV	Low heating value
LP	Low-pressure
LPOP	Levelized profit of Portland clinker precursor
LPST	Low-pressure steam turbine
MC	Maintenance cost
MSR	Methanol synthesis reactor
NPV	Net present value
OC	Operator's costs
OCC	Owner's cost and contingency
PC	Process contingency
PSA	Pressure swing adsorption
RB	Reboiler
SH	Superheater
TDC	Total direct cost
TEA	Techno-economic analysis

(*continued on next page*)

(*continued*)

HP	High-pressure	TEC	Total equipment cost
HPST	High-pressure steam turbine	TI	Total income
HRSG	Heat recovery steam generator	TIC	Total installation cost
IC	Indirect cost	TO	Total opex
IP	Intermediate-pressure	TPC	Total plant cost
IPST	Intermediate-pressure steam turbine	VO	Variable opex

Data availability

Data will be made available on request.

References

ACA, 2025. How Cement is Made. https://www.cement.org/cementconcrete/how-cement-is-made.

Ahmadullah, A.B., Rahimi, M.A., Ulfat, D.S., Irshad, A.S., Doost, Z.H., Wali, N., Karimi, B. A., 2025. Decarbonizing Afghanistan: the most cost-effective renewable energy system for hydrogen production. Energy 324. https://doi.org/10.1016/j.energy.2025.136000.

Amiri, A., Vaseghi, M.R., 2015. Waste heat recovery power generation systems for cement production process. IEEE Trans. Ind. Appl. 51 (1), 13–19. https://doi.org/10.1109/tia.2014.2347196.

Bacatelo, M., Capucha, F., Ferrão, P., Margarido, F., 2023. Selection of a CO_2 capture technology for the cement industry: an integrated TEA and LCA methodological framework. J. CO2 Util. 68, 102375. https://doi.org/10.1016/j.jcou.2022.102375.

Boháč, M., Kubátová, D., Krejčí Kotlánová, M., Khongová, I., Zezulová, A., Novotný, R., Palou, M.T., Staněk, T., Všianský, D., 2022. The role of Li_2O, MgO and CuO on SO_3 activated clinkers. Cement Concr. Res. 152, 106672. https://doi.org/10.1016/j.cemconres.2021.106672.

Bourtsalas, A.C., Zhang, J., Castaldi, M.J., Themelis, N.J., Karaiskakis, A.N., 2018. Use of non-recycled plastics and paper as alternative fuel in cement production. J. Clean. Prod. 181, 8–16. https://doi.org/10.1016/j.jclepro.2018.01.214.

Buli, N., 2025. Heidelberg sells out of net-zero cement from Norway plant, CEO says. Available at: https://www.reuters.com/sustainability/climate-energy/heidelberg-sells-out-net-zero-cement-norway-plant-ceo-says-2025-06-18/?utm_source. January 2026.

Chen, H., Ma, X., Dai, H., 2010. Reuse of water purification sludge as raw material in cement production. Cem. Concr. Compos. 32 (6), 436–439. https://doi.org/10.1016/j.cemconcomp.2010.02.009.

Detz, R.J., Reek, J.N.H., van der Zwaan, B.C.C., 2018. The future of solar fuels: when could they become competitive? Energy Environ. Sci. 11 (7), 1653–1669. https://doi.org/10.1039/c8ee00111a.

Di, Z., Lei, F., Jing, J., Peng, H., Lu, X., Cheng, F., 2024. Technical alternatives for coke oven gas utilization in China: a comparative analysis of environment-economic-strategic perspectives. Environ. Sci. Ecotechnol. 21, 100395. https://doi.org/10.1016/j.ese.2024.100395.

Díez, E., Langston, P., Ovejero, G., Romero, M.D., 2009. Economic feasibility of heat pumps in distillation to reduce energy use. Appl. Therm. Eng. 29 (5-6), 1216–1223. https://doi.org/10.1016/j.applthermaleng.2008.06.013.

EEAS, 2025. Carbon border adjustment mechanism. Available at: https://www.eeas.europa.eu/delegations/china/carbon-border-adjustment-mechanism_en?utm_source. January 2026.

Ellis, L.D., Badel, A.F., Chiang, M.L., Park, R.J.-Y., Chiang, Y.-M., 2020. Toward electrochemical synthesis of cement-An electrolyzer-based process for decarbonating $CaCO_3$ while producing useful gas streams. Proc. Natl. Acad. Sci. USA 117 (23), 12584–12591. https://doi.org/10.1073/pnas.1821673116.

Gallego Dávila, J., Sacchi, R., Pizzol, M., 2023. Preconditions for achieving carbon neutrality in cement production through CCUS. J. Clean. Prod. 425, 138935. https://doi.org/10.1016/j.jclepro.2023.138935.

Giardini, A.A., Salotti, C.A., Lakner, J.F., 1968. Synthesis of graphite and hydrocarbons by reaction between calcite and hydrogen. Science 159, 317–319. https://doi.org/10.1126/science.159.3812.317.

Goncharov, A., Zhutovsky, S., 2022. Eco-friendly belite cement from crude calcareous oil shale with low calorific value. Cement Concr. Res. 159, 106874. https://doi.org/10.1016/j.cemconres.2022.106874.

GTAIC, 2025. Cement markets in Europe 2025: cement import dynamics, prices, competition. Available at: https://gtaic.ai/market-reports/cement-markets-europe-2025?utm_source. January 2026.

Gubin, V., Kadlez, D., Bartik, A., Steiner, L., Zeitlhofer, J., Thelen, F., Hofbauer, H., Müller, S., 2025. Hydrogen production from woody biomass via fixed-bed gasification at pilot-scale. Int. J. Hydrogen Energy 114, 462–474. https://doi.org/10.1016/j.ijhydene.2025.02.357.

Haaf, M., Anantharaman, R., Roussanaly, S., Ströhle, J., Epple, B., 2020. CO_2 capture from waste-to-energy plants: Techno-economic assessment of novel integration concepts of calcium looping technology. Resour. Conserv. Recycl. 162, 104973. https://doi.org/10.1016/j.resconrec.2020.104973.

Her, S., Park, J., Li, P., Bae, S., 2022. Feasibility study on utilization of pulverized eggshell waste as an alternative to limestone in raw materials for Portland cement clinker production. Constr. Build. Mater. 324, 126589. https://doi.org/10.1016/j.conbuildmat.2022.126589.

Hills, T., Leeson, D., Florin, N., Fennell, P., 2016. Carbon capture in the cement industry: technologies, progress, and retrofitting. Environ. Sci. Technol. 50 (1), 368–377. https://doi.org/10.1021/acs.est.5b03508.

Hou, G., Chen, J., Lu, B., Chen, S., Cui, E., Naguib, H.M., Guo, M.-Z., Zhang, Q., 2020. Composition design and pilot study of an advanced energy-saving and low-carbon rankinite clinker. Cement Concr. Res. 127. https://doi.org/10.1016/j.cemconres.2019.105926.

Hu, Y., Ahn, H., 2017. Process integration of a Calcium-looping process with a natural gas combined cycle power plant for CO_2 capture and its improvement by exhaust gas recirculation. Appl. Energy 187, 480–488. https://doi.org/10.1016/j.apenergy.2016.11.014.

Huang, M., Ying, X., Shen, D., Feng, H., Li, N., Zhou, Y., Long, Y., 2017. Evaluation of oil sludge as an alternative fuel in the production of Portland cement clinker. Constr. Build. Mater. 152, 226–231. https://doi.org/10.1016/j.conbuildmat.2017.06.157.

HyIron, 2023. Opening of the hydrogen direct reduction plant in Lingen by Lower Saxony's Environment and Energy Minister Meyer. Available at: https://hyiron.com/opening-of-the-hydrogen-direct-reduction-plant-in-lingen-by-lower-saxonys-environment-and-energy-minister-meyer/?utm_source. January 2026.

IEA, 2025. Demand and supply measures for the steel and cement transition. Available at: https://www.iea.org/reports/demand-and-supply-measures-for-the-steel-and-cement-transition. January 2026.

Jacob, R.M., Tokheim, L.-A., 2023. Electrified calciner concept for CO_2 capture in pyro-processing of a dry process cement plant. Energy 268, 126673. https://doi.org/10.1016/j.energy.2023.126673.

Jiang, P., Li, L., Zhao, G., Zhang, H., Ji, T., Mu, L., Lu, X., Zhu, J., 2023. Reductive calcination of calcium carbonate in hydrogen and methane: a thermodynamic analysis on different reaction routes and evaluation of carbon dioxide mitigation potential. Chem. Eng. Sci. 276, 118823. https://doi.org/10.1016/j.ces.2023.118823.

Karpan, B., Abdul Raman, A.A., Rahim, R., Aroua, M.K.T., Buthiyappan, A., 2022. Carbon footprint evaluation of industrial wastes based solid fuel in the context of its use in a cement plant. Waste Biomass Valor. 13 (8), 3723–3735. https://doi.org/10.1007/s12649-022-01761-6.

Kawabata, M., Kurata, O., Iki, N., Tsutsumi, A., Furutani, H., 2013. System modeling of exergy recuperated IGCC system with pre- and post-combustion CO_2 capture. Appl. Therm. Eng. 54 (1), 310–318. https://doi.org/10.1016/j.applthermaleng.2013.01.029.

Kiss, A.A., Flores Landaeta, S.J., Infante Ferreira, C.A., 2012. Towards energy efficient distillation technologies–making the right choice. Energy 47 (1), 531–542. https://doi.org/10.1016/j.energy.2012.09.038.

Kiss, A.A., Pragt, J.J., Vos, H.J., Bargeman, G., de Groot, M.T., 2016. Novel efficient process for methanol synthesis by CO_2 hydrogenation. Chem. Eng. J. 284, 260–269. https://doi.org/10.1016/j.cej.2015.08.101.

Ma, R., Li, J., Zhang, X., Jia, P., Liu, Z., Wu, J., Feng, F., Xin, W., 2024. Decomposition of monazite in Bayan Obo rare earth ore by roasting of Na_2CO_3 pellets. J. Rare Earths 42 (10), 1969–1978. https://doi.org/10.1016/j.jre.2023.09.014.

Magli, F., Spinelli, M., Fantini, M., Romano, M.C., Gatti, M., 2022. Techno-economic optimization and off-design analysis of CO_2 purification units for cement plants with oxyfuel-based CO_2 capture. Int. J. Greenh. Gas Control 115. https://doi.org/10.1016/j.ijggc.2022.103591.

Mamun, A.A., Talukder, M.A., 2024. Techno-economic analysis of the direct solar conversion of carbon dioxide into renewable fuels. Energy Convers. Manag. 321. https://doi.org/10.1016/j.enconman.2024.119038.

Marenco-Porto, C.A., Fierro, J.J., Nieto-Londoño, C., Lopera, L., Escudero-Atehortua, A., Giraldo, M., Jouhara, H., 2023. Potential savings in the cement industry using waste heat recovery technologies. Energy 279, 127810. https://doi.org/10.1016/j.energy.2023.127810.

Matsuzawa, K., Atarashi, D., Miyauchi, M., Sakai, E., 2017. Interactions between fluoride ions and cement paste containing superplasticizer. Cement Concr. Res. 91, 33–38. https://doi.org/10.1016/j.cemconres.2016.10.006.

Montes-Hernandez, G., 2025. Decarbonizing the cement industry is crucial for reducing CO_2 emissions: myth or reality? Chem. Eng. J. 518. https://doi.org/10.1016/j.cej.2025.164995.

Nawaz, Z., Ali, U., 2020. Techno-economic evaluation of different operating scenarios for indigenous and imported coal blends and biomass co-firing on supercritical coal fired power plant performance. Energy 212. https://doi.org/10.1016/j.energy.2020.118721.

NDRC, 2022. Hydrogen industry development Medium- and long-term plan (2021–2035). Available at: https://www.ndrc.gov.cn/xxgk/zcfb/ghwb/20220323/t20220323_1320038.html?utm_source. January 2026.

Nikulshina, V., Halmann, M., Steinfeld, A., 2009. Coproduction of syngas and lime by combined $CaCO_3$-Calcination and CH_4-Reforming using a particle-flow reactor driven by concentrated solar radiation. Energy Fuel. 23 (12), 6207–6212. https://doi.org/10.1021/ef9007246.

Okoji, A.I., Anozie, A.N., Omoleye, J.A., Taiwo, A.E., Osuolale, F.N., 2022. Energetic assessment of a precalcining rotary kiln in a cement plant using process simulator and neural networks. Alex. Eng. J. 61 (7), 5097–5109. https://doi.org/10.1016/j.aej.2021.10.010.

Okolie, J.A., Nanda, S., Dalai, A.K., Kozinski, J.A., 2021. Techno-economic evaluation and sensitivity analysis of a conceptual design for supercritical water gasification of soybean straw to produce hydrogen. Bioresour. Technol. 331, 125005. https://doi.org/10.1016/j.biortech.2021.125005.

Pardo, N., Moya, J.A., Mercier, A., 2011. Prospective on the energy efficiency and CO_2 emissions in the EU cement industry. Energy 36 (5), 3244–3254. https://doi.org/10.1016/j.energy.2011.03.016.

Park, Y., Ju, Y., Park, D., Lee, C.-H., 2016. Adsorption equilibria and kinetics of six pure gases on pelletized zeolite 13X up to 1.0 MPa: CO_2, CO, N_2, CH_4, Ar and H_2. Chem. Eng. J. 292, 348–365. https://doi.org/10.1016/j.cej.2016.02.046.

Peng, D.-Y., Robinson, D.B., 1976. A new two-constant equation of State. Ind. Eng. Chem. Fundam. 15 (1), 59–64. https://doi.org/10.1021/i160057a011.

Puig-Gamero, M., Argudo-Santamaria, J., Valverde, J.L., Sánchez, P., Sanchez-Silva, L., 2018. Three integrated process simulation using aspen plus®: pine gasification, syngas cleaning and methanol synthesis. Energy Convers. Manag. 177, 416–427. https://doi.org/10.1016/j.enconman.2018.09.088.

Reller, A., Padeste, C., Hug, P., 1987. Formation of organic carbon compounds from metal carbonates. Nature 329, 527–529. https://doi.org/10.1038/329527a0.

Romano, M.C., 2013. Ultra-high CO_2 capture efficiency in CFB oxyfuel power plants by calcium looping process for CO_2 recovery from purification units vent gas. Int. J. Greenh. Gas Control 18, 57–67. https://doi.org/10.1016/j.ijggc.2013.07.002.

Ryu, G.U., Kim, H.J., Yu, H.J., Pyo, S., 2024. Utilization of steelmaking slag in cement clinker production: a review. J. CO2 Util. 84, 102842. https://doi.org/10.1016/j.jcou.2024.102842.

Sanaye, S., Khakpaay, N., Chitsaz, A., Hassan Yahyanejad, M., Zolfaghari, M., 2020. A comprehensive approach for designing, modeling and optimizing of waste heat recovery cycle and power generation system in a cement plant: a thermo-economic and environmental assessment. Energy Convers. Manag. 205, 112353. https://doi.org/10.1016/j.enconman.2019.112353.

Shao, B., Zhu, Y., Hu, J., Zong, Y., Xie, Z., Li, S., Du, W., Wang, M., Liu, H., Qian, F., 2024. Chemical engineering solution for carbon neutrality in cement industry: Tailor a pathway from inevitable CO_2 emission into syngas. Chem. Eng. J. 483, 149098. https://doi.org/10.1016/j.cej.2024.149098.

Siskos, C., Manakas, P., Karaoglanoglou, L., Vlysidis, A., 2026. Techno-economic and environmental analysis of methanol production from cement carbon dioxide emissions. Renew. Energy 256. https://doi.org/10.1016/j.renene.2025.124109.

Sun, S., Chen, Z., Xu, Y., Wang, Y., Zhang, Y., Dejoie, C., Xu, S., Xu, X., Wu, C., 2024. Potassium-Promoted Limestone for preferential direct hydrogenation of carbonates in integrated CO_2 capture and utilization. JACS Au 4 (1), 72–79. https://doi.org/10.1021/jacsau.3c00403.

Taylor, H.F.W., 1997. Cement Chemistry, second ed. Thomas Telford Ltd, London.

Tsakiridis, P.E., Samouhos, M., Peppas, A., Katsiotis, N.S., Velissariou, D., Katsiotis, M.S., Beazi, M., 2016. Silico-aluminous bottom ash valorisation in cement clinker production: synthesis, characterization and hydration properties. Constr. Build. Mater. 126, 673–681. https://doi.org/10.1016/j.conbuildmat.2016.09.089.

Tsakiridis, P.E., Samouhos, M., Perraki, M., 2017. Valorization of Dried Olive Pomace as an alternative fuel resource in cement clinkerization. Constr. Build. Mater. 153, 202–210. https://doi.org/10.1016/j.conbuildmat.2017.07.102.

Wang, I., Li, D., Wang, S., Wang, Y., Lin, G., Yan, B., Li, Z., 2023. Limestone hydrogenation combined with reverse water–gas shift reaction under fluidized and iso-thermal conditions using MFB-TGA-MS. Chem. Eng. J. 472, 144822. https://doi.org/10.1016/j.cej.2023.144822.

Wang, Q., Li, J., Zhu, X., Yao, G., Wu, P., Wang, Z., Lyu, X., Hu, S., Qiu, J., Chen, P., Wang, J., 2020. Approach to the management of gold ore tailings via its application in cement production. J. Clean. Prod. 269, 122303. https://doi.org/10.1016/j.jclepro.2020.122303.

Wang, Y., Wen, Z., Xu, M., Kosajan, V., 2024a. The carbon-energy-water nexus of the carbon capture, utilization, and storage technology deployment schemes: a case study in China's cement industry. Appl. Energy 362, 122991. https://doi.org/10.1016/j.apenergy.2024.122991.

Wang, Y., Yang, M., Shen, F., Zhou, M., Du, W., 2024b. Conceptual design and life-cycle environmental and economic assessment of low-carbon cement manufacturing processes. J. Clean. Prod. 471, 143349. https://doi.org/10.1016/j.jclepro.2024.143349.

Williams, F., Yang, A., 2024. Potential of reducing CO_2 emissions in cement production through altering clinker compositions. Ind. Eng. Chem. Res. 63 (40), 17158–17167. https://doi.org/10.1021/acs.iecr.4c01885.

Williams, F., Yang, A., Nhuchhen, D.R., 2024. Decarbonisation pathways of the cement production process via hydrogen and oxy-combustion. Energy Convers. Manag. 300, 117931. https://doi.org/10.1016/j.enconman.2023.117931.

Wu, N., Lan, K., Yao, Y., 2023. An integrated techno-economic and environmental assessment for carbon capture in hydrogen production by biomass gasification. Resour. Conserv. Recycl. 188, 106693. https://doi.org/10.1016/j.resconrec.2022.106693.

Wu, Y., Chen, X., Ma, J., Wu, Y., Liu, D., Mi, J., Xie, W., 2020. System integration for coal-fired power plant with post combustion CO_2 capture: comparative study for different solid dry sorbents. Fuel 280. https://doi.org/10.1016/j.fuel.2020.118561.

Xu, M., Hu, L., Zhao, Q., Dong, Z., Mo, L., 2025. Effects of fluorite tailings content on formation, properties and fluorine doping preferences of high-silica clinker: experimental study and industrial verification. J. Build. Eng. 106. https://doi.org/10.1016/j.jobe.2025.112612.

Xue, Z., Guo, J., Wu, S., Xie, W., Fu, Y., Zhao, X., Fan, K., Xu, M., Yan, H., Shao, M., Duan, X., 2023. Co-thermal in-situ reduction of inorganic carbonates to reduce carbon-dioxide emission. Sci. China Chem. 66 (4), 1201–1210. https://doi.org/10.1007/s11426-022-1537-6.

Yu, S., Guo, J., Xu, M., Zhang, W., Guo, D., Wang, Y., Xue, Z., Yan, H., Yang, Y., Fang, J., Shao, M., Duan, X., 2025. In situ reduction of Fe-Doped calcium carbonate to perform low-carbon cement clinker coupling with generation of syngas. ACS Catal. 15 (18), 16132–16143. https://doi.org/10.1021/acscatal.5c03469.

Yuan, W., 2019. Chemical Engineering Handbook, third ed. Chemical Industry Press, Beijing.

Zhang, D., Li, H., Wu, Q., Yang, G., Wang, H.-F., Cao, Y., Wang, H., Yang, S., Yu, H., 2024a. Techno-economic analysis of hydrogen-driven calcium looping process for flue gas decarbonization. Carbon Future 1 (4), 9200023. https://doi.org/10.26599/cf.2024.9200023.

Zhang, D., Li, H., Yang, G., Wang, H.-F., Cao, Y., Wang, H., Yu, H., 2024b. Hydrogen-driven routes to steel from siderite with low CO_2 emissions: a modeling study. Chem. Eng. Sci. 287, 119702. https://doi.org/10.1016/j.ces.2024.119702.

Zhang, Y., Shen, J., Zeng, Y., Tian, X., Ding, M., 2025. Direct reduction of calcium carbonate by coupling with methane dry reforming using NiO/S-1 as catalyst. Sep. Purif. Technol. 354, 128816. https://doi.org/10.1016/j.seppur.2024.128816.

Zhang, Z., Mowbray, B.A.W., Parkyn, C.T.E., Waizenegger, C., Williams, A.S.R., Lees, E. W., Ren, S., Kim, Y., Jansonius, R.P., Berlinguette, C.P., 2022. Cement clinker precursor production in an electrolyser. Energy Environ. Sci. 15 (12), 5129–5136. https://doi.org/10.1039/d2ee02349k.